



**Universidade do Minho**  
**Escola de Engenharia**

Cátia Sofia Costa da Silva

**Development of an aptamer-based  
nanoparticle towards breast cancer**

Dissertação de Mestrado

Mestrado em Biotecnologia

Trabalho efetuado sob a orientação da

**Professora Doutora Lígia Raquel Marona Rodrigues**

setembro 2018

DECLARAÇÃO

Nome

\_\_\_\_\_

Endereço eletrónico: \_\_\_\_\_ Telefone: \_\_\_\_\_ /

\_\_\_\_\_

Número do Bilhete de Identidade: \_\_\_\_\_

Título dissertação /tese

\_\_\_\_\_

\_\_\_\_\_

\_\_\_\_\_

Orientador(es):

\_\_\_\_\_

\_\_\_\_\_ Ano de conclusão: \_\_\_\_\_

Designação do Mestrado:

\_\_\_\_\_

DE ACORDO COM A LEGISLAÇÃO EM VIGOR, NÃO É PERMITIDA A REPRODUÇÃO DE QUALQUER  
PARTE DESTA TESE/TRABALHO

Universidade do Minho, \_\_\_/\_\_\_/\_\_\_\_\_

Assinatura: \_\_\_\_\_

## AKNOWLEDGMENTS

Gostaria de expressar o meu agradecimento à minha orientadora, Professora Lígia Rodrigues, pela oportunidade que me deu de ingressar neste projeto e pela disponibilidade, orientação, confiança e todos os conselhos desde a UC Projecto até ao final da Dissertação

Agradeço também à Débora Ferreira por me ter acompanhado nesta jornada: por todas as horas de citometria, conselhos, apoio e disponibilidade. Obrigada por partilhares o teu conhecimento, tempo e experiência.

Um agradecimento especial à Ana Luísa Carvalho e à Rute Tavares por todas as horas que passamos juntas, dentro e fora do laboratório. Ainda bem que vos conheci.

Um agradecimento a todos os colegas do LBBS. Tornaram a passagem por este laboratório uma fase especial e descontraída.

Por último, mas não menos importante, um agradecimento aos meus pais, à minha irmã e ao meu namorado. Obrigado por me ouvirem e me apoiarem ao longo deste ano. Obrigado por estarem sempre do meu lado e me motivarem. O vosso carinho e o vosso amor foram sempre o meu pilar.

Agradeço a todos aqueles que, direta ou indiretamente, contribuíram para a realização deste trabalho.



## ABSTRACT

Breast cancer is a heterogeneous and complex disease which incidence is increasing. Diagnosis of breast cancer evolved in the past from morphological observation to mammography. Immunopathological and high-throughput methods are recent methods that allow distinguishing different breast cancer types. The biomarkers used for diagnosis include estrogen receptor, progesterone receptor and human epidermal growth factor receptor 2. Triple negative breast cancer lacks the expression of both ER and PR, as well as the over-expression and/or lack of the HER2 gene amplification. TNBCs diagnosis and therapy are challenging due to lack of known receptors. However, many efforts are being developed to overcome these hurdles. One of those include the use of aptamers that are single-stranded oligonucleotides able to bind various molecular targets with high affinity and specificity and in some cases able to penetrate tumours. Hence, it is possible to develop aptamers that specifically recognize tumour cell receptors. The main aim of this work was to develop an aptamer-nanoparticle complex for TNBC early diagnosis. In the current project, the secondary structure of two previously selected aptamers by Cell-SELEX, aptamer #1 and aptamer #2, were predicted using Mfold, which suggested the formation of a hairpin at 4 °C and 37 °C. Then, the binding ability of these aptamers was assessed by flow cytometry and microscopy, revealing that aptamer #1 and aptamer #2 specifically bound to MDA-MB-231 and not to MCF-10-2A cells. Furthermore, the dissociation constants of both aptamers were calculated, aptamer #1  $K_D = 82.29 \pm 13.64$  nM and aptamer #2  $K_D$  was  $54.63 \pm 18.87$  nM. Aptamer #2  $K_D$  was found to be lower, although the differences are not statistically significant. The cytotoxic assay indicated that the aptamers affected MDA-MB-231 cells, although the morphological assay pointed in a different direction. Moreover, amine labeled aptamer was used to functionalize green fluorescent silica particles using the carbodiimide chemistry, and the ligation aptamer-particle was evaluated through three different methodologies including Dynamic Light Scattering, NanoDrop and gel electrophoresis. The functionalization was not successful. However, binding ability assays were performed and suggested that only silica nanoparticles entered the cells, possibly through endocytosis. In addition, the possible targets for these aptamers were ascertain and it was found that 4 possible targets are present in MDA-MB-231. It was shown that the target is present in the cell membrane and in the cytosol. Although an aptamer-based nanoparticle for diagnostic was not achieved, improvements towards achieving this goal can be done.



## SUMÁRIO

O cancro da mama é uma doença heterogénea e complexa cuja incidência está a aumentar. O diagnóstico de cancro da mama evoluiu desde a observação morfológica até à mamografia. Métodos imunopatológicos e de alto rendimento são métodos recentes e permitem distinguir diferentes tipos de cancro da mama. Os biomarcadores utilizados para o diagnóstico incluem recetor de estrogénio, recetor de progesterona e recetor do fator de crescimento epidérmico humano 2. O cancro da mama triplo negativo não possui a expressão de recetores de estrogénio e progesterona, assim como a sobreexpressão e / ou falta de amplificação do gene recetor do fator de crescimento epidérmico humano 2, tornando o diagnóstico e a terapia desafiantes, sendo feitos muitos esforços nesse sentido. Um deles inclui o uso de aptamers que são oligonucleotídeos de cadeia simples capazes de se ligar a vários alvos moleculares com alta afinidade e especificidade e, em alguns casos, capazes de penetrar em tumores. Assim, é possível desenvolver aptamers que reconhecem especificamente recetores de células tumorais. O principal objetivo deste trabalho foi desenvolver um complexo aptamers-nanopartícula para o diagnóstico precoce do cancro da mama triplo negativo. Neste projeto, a estrutura secundária de aptamer # 1 e aptamer # 2 previamente selecionados por Cell-SELEX foi prevista usando Mfold, o que sugeriu a formação de um hairpin a 4 °C e 37 °C. Em seguida, a capacidade de ligação destes aptamers foi avaliada por citometria de fluxo e microscopia, revelando que os aptamers # 1 e # 2 ligaram-se especificamente a MDA-MB-231 e não a MCF-10-2A. Além disso, as constantes de dissociação de ambos os aptamers foram calculadas: aptamer # 1  $K_D = 82,29 \pm 13,64$  nM e aptamer # 2  $K_D$  foi  $54,63 \pm 18,87$  nM. A  $K_D$  # 2 é menor que a  $K_D$  # 1, embora a diferença não seja estatisticamente significativa. O ensaio citotóxico indicou que os aptamers afetavam as células MDA-MB-231, embora o ensaio morfológico apontasse em uma direção diferente. Além disso, o aptamer marcado com amina foi utilizado para funcionalizar nanopartículas de sílica fluorescentes através da química da carbodiimida; a ligação de partículas de aptamers foi avaliada através de três metodologias diferentes, incluindo Dynamic Light Scattering, NanoDrop e eletroforese em gel. A funcionalização não foi bem sucedida. Os ensaios de capacidade de ligação foram realizados e sugeriram que as nanopartículas de sílica entraram nas células, possivelmente através de endocitose. Encontraram-se 4 alvos possíveis presentes em MDA-MB-231. Foi demonstrado que o alvo está presente na membrana celular e no citosol. Embora uma nanopartícula dirigida para diagnóstico não tenha sido obtida, melhorias para atingir essa meta podem ser feitas.





## TABLE OF CONTENTS

AKNOWLEDGMENTS .....	iii
ABSTRACT .....	v
SUMÁRIO .....	vii
TABLE OF CONTENTS .....	ix
LIST OF FIGURES .....	xiii
LIST OF TABLES .....	xvii
LIST OF ABBREVIATIONS .....	xix
MOTIVATION AND AIM OF THE PROJECT .....	xxi
CHAPTER 1. INTRODUCTION .....	1
1.1 Triple Negative Breast Cancers (TNBC) .....	4
1.1.1 TNBC Subtypes .....	4
1.1.2 TNBC Screening .....	6
1.1.3 TNBC Treatments .....	8
1.2 Aptamers .....	9
1.2.1 Aptamers in cancer diagnosis .....	12
1.2.2 Aptamers in cancer treatment .....	14
1.3 Nanoparticles .....	17
1.3.1 Liposomes .....	17
1.3.2 Magnetic nanoparticles .....	18
1.3.3 Silica Nanoparticles .....	20
CHAPTER 2. MATERIALS AND METHODS .....	23
Cell Lines.....	25
2.1 Folding prediction .....	26
2.2 <i>In vitro</i> studies .....	26
Fluorescence Microscopy .....	26
Flow Cytometry .....	26
Membrane pre-treatment .....	27

TABLE OF CONTENTS

2.2.1 Determination of the Dissociation Constant ( $K_D$ ) .....	28
2.2.2 Cytotoxicity .....	28
Toxicity assay .....	28
2.2.3 Morphology Assay .....	29
<b>2.3 Biotin and Amine labeled Aptamer .....</b>	<b>29</b>
2.3.1 Polymerase Chain Reaction (PCR) .....	29
Gel Electrophoresis .....	30
2.3.2 Lambda Exonuclease .....	30
2.3.2.1 Aptamer purification .....	31
Approach 1: Phenol/Chloroform DNA extraction .....	31
Approach 2: Zymoclean Gel DNA Recovery Kit .....	31
Approach 3: Zymoclean DNA Clean & Concentrator Kit .....	32
2.3.3 Bioconjugation .....	32
2.3.3.1 Characterization of the conjugated aptamer-nanoparticles .....	33
Flow Cytometry .....	33
Dynamic Light Scattering .....	33
Microvolume Spectrophotometry and Fluorometry .....	33
2.3.4 Aptamer –mediated pull-down assay .....	34
2.3.4.1 Subcellular fractioning .....	34
Membrane and Cytosolic fractions isolation .....	34
Nuclear fraction isolation .....	35
Protein Quantification through Bradford Protein Assay .....	35
2.3.4.2 Aptamer-target binding assay .....	35
<b>CHAPTER 3. RESULTS AND DISCUSSION .....</b>	<b>37</b>
<b>3.1 Secondary structure .....</b>	<b>39</b>
<b>3.2 <i>In vitro</i> studies .....</b>	<b>42</b>
3.2.1 $K_D$ determination using flow cytometry .....	48

<b>3.3 Biotin and amine labeled aptamers .....</b>	<b>49</b>
3.3.1 Aptamer-based pull-down .....	50
3.3.2 Cytotoxicity evaluation .....	55
3.3.3 Morphology assay .....	55
3.3.4 Bioconjugation .....	57
3.3.4.1 Characterization of aptamer-nanoparticle conjugates .....	57
3.3.4.2 Binding .....	59
<b>CHAPTER 4: CONCLUSIONS AND RECOMENDATIONS FOR FUTURE WORK .....</b>	<b>63</b>
<b>REFERENCES .....</b>	<b>67</b>
<b>APPENDIXES .....</b>	<b>81</b>



## LIST OF FIGURES

### CHAPTER 1: INTRODUCTION

<b>Figure 1.1.</b> MDA-MB-231 cell line in low (left) and high (right) density. (from American Type Culture Collection) .....	6
<b>Figure 1.2.</b> Schematic representation of the SELEX process (Prakash & Rajamanickam, 2015) .....	11

### CHAPTER 3: RESULTS AND DISCUSSION

<b>Figure 3.1.</b> Flow cytometry binding assay using MDA-MB-231 cells for (A) aptamer #1 and (B) aptamer #2. Comparison between control, incubation at 37 °C, 4 °C and pre-treatment with trypsin and proteinase K. ns $P > 0.05$ ; * $P \leq 0.05$ ; ** $P \leq 0.01$ ; *** $P \leq 0.001$ ; **** $P \leq 0.0001$ . The results are the average of % fluorescent cells for each treatment $\pm$ standard deviation .....	43
<b>Figure 3.2.</b> Flow cytometry binding assay with MDA-MB-231 for library. Comparison between control, aptamer #1, aptamer #2 and library. ns $P > 0.05$ ; * $P \leq 0.05$ ; ** $P \leq 0.01$ ; *** $P \leq 0.001$ ; **** $P \leq 0.0001$ . The results are the average of % fluorescent cells for each treatment $\pm$ standard deviation .....	45
<b>Figure 3.3.</b> Flow cytometry binding assay for MCF-10-2A. The cells were incubated with aptamer #1, aptamer #2 and library. ns $P > 0.05$ ; * $P \leq 0.05$ ; ** $P \leq 0.01$ ; *** $P \leq 0.001$ ; **** $P \leq 0.0001$ . The results are the average of % fluorescent cells for each treatment $\pm$ standard deviation .....	46
<b>Figure 3.4.</b> Fluorescence microscopy images of MDA-MB-231 cells incubated with aptamer #1 (A and B), aptamer #2 (C and D) and library (E and F). (A, C, E) Blue: nuclei stained with DAPI; (B, D, F) Green: represent cells stained with fluorescent aptamer .....	47
<b>Figure 3.5.</b> Kinetics curve of (A) aptamer #1 and (B) aptamer #2 and their respective $K_D$ . Flow cytometry was used to determine the binding affinities of the aptamers selected against MDA-MB-231 cells .....	48
<b>Figure 3.6.</b> Gel agarose from digestion of ds aptamer #1 to ss aptamer #1 and subsequent extraction through phenol/chloroform and purification with ethanol .....	50

LIST OF FIGURES

**Figure 3.7.** SDS-PAGE gel from pull-down assay from nuclei fraction. (1) Biomarker, (2) nuclear fraction, (3) nuclear fraction incubated with aptamer #2 at 37 °C, (4) nuclear fraction incubated with aptamer #2 at 4 °C ..... 52

**Figure 3.8.** SDS-PAGE gels from pull-down assay from (A) cytosolic fraction and (B) membrane fraction of MDA-MB-231. A: (1) Biomarker, (2) cytosol fraction, (4) cytosol fraction incubated with aptamer #1 at 37 °C, (5) cytosol fraction incubated with aptamer #1 at 4 °C, (6) cytosol fraction incubated with aptamer #2 at 37 °C, (7) cytosol fraction incubated with aptamer #2 at 4 °C. B: (1) Biomarker, (2) membrane fraction, (3) membrane fraction incubated with aptamer #1 at 37 °C, (4) membrane fraction incubated with aptamer #1 at 4 °C, (5) membrane fraction incubated with aptamer #2 at 37 °C, (6) membrane fraction incubated with aptamer #2 at 4 °C ..... 53

**Figure 3.9.** SRB assay for MDA-MB-231 cells. ns  $P > 0.05$ ; \*  $P \leq 0.05$ ; \*\*  $P \leq 0.01$ ; \*\*\*  $P \leq 0.001$ ; \*\*\*\*  $P \leq 0.0001$ . The results are the average of % fluorescent cells for each treatment  $\pm$  standard deviation ..... 55

**Figure 3.10.** Morphology assay for MDA-MB-231 incubated with no aptamer, with aptamer #1 and aptamer #2 at 0h, 3h, 6h, 8h and 24h after incubation ..... 56

**Figure 3.11.** Gel electrophoresis to confirm the functionalization of aptamer displaying (1) biomarker, (2) aptamer #1 conjugated with SiNPs, (3) aptamer #2 conjugated with SiNPs and (4) SiNPS ..... 58

**Figure 3.12.** Flow cytometry for MDA-MB-231 cells incubated with aptamer #1 conjugated, aptamer #2 conjugated and free SiNPs. ns  $P > 0.05$ ; \*  $P \leq 0.05$ ; \*\*  $P \leq 0.01$ ; \*\*\*  $P \leq 0.001$ ; \*\*\*\*  $P \leq 0.0001$ . The results are the average of % fluorescent cells for each treatment  $\pm$  standard deviation ..... 59

**Figure 3.13.** Fluorescence microscopy of MDA-MB-231 cells incubated with aptamer #1 (A and B), aptamer #2 (C and D) and library (E and F). (A, C, E) Blue, nuclei stained with DAPI, (B, D, F). Green, represents cells stained with fluorescent aptamer ..... 60

APPENDIXES

**Figure A.1** Calibration curve of Bradford Protein Assay.  $y = 0,7132x + 0,0657$ ;  $R^2 = 0,9607$  83

**Figure A.2** Aptamer #1 mediated pull down assay of membrane fraction using Binding Buffer containing FBS and BSA. (1) Biomarker, (2 and 6) membrane fraction, (3) membrane fraction incubated with beads, (4) membrane fraction incubated with aptamer at 4 °C and (5) membrane fraction incubated with aptamer at 37 °C ..... 83

**Figure A.3** Aptamer #1 mediated pull-down assay of (A) nuclear, mitochondrial, (B) cytosolic and membrane fraction using Binding Buffer containing FBS. A: (1) Biomarker, (2) nuclear fraction, (3) nuclear fraction incubated with beads, (4) nuclear fraction incubated with aptamer at 4 °C, (5) nuclear fraction incubated with aptamer at 37 °C, (6) mitochondrial fraction, (7) mitochondrial fraction incubated with beads, (8) mitochondrial fraction incubated with aptamer at 4 °C, (9) mitochondrial fraction incubated with aptamer at 37 °C. B (1) Biomarker, (2) cytosol fraction, (3) cytosol fraction incubated with beads, (4) cytosol fraction incubated with aptamer at 4 °C, (5) cytosol fraction incubated with aptamer at 37 °C, (6) membrane fraction, (7) membrane fraction incubated with beads, (8) membrane fraction incubated with aptamer at 4 °C, (9) membrane fraction incubated with aptamer at 37 °C and (10) Biomarker ..... 84





## LIST OF TABLES

### CHAPTER 1: INTROCUCTION

Table 1.1. Summary of Triple negative breast cancer subtypes and its main characteristics.....	5
--	---

### CHAPTER 2: MATERIALS AND METHODS

Table 2.1 PCR Master Mix for 1 PCR reaction tube for both aptamer #1 and aptamer #2....	29
---	----

### CHAPTER 3: RESULTS AND DISCUSSION

Table 3.1- List of the aptamers selected against MDA-MB-231 cell line that display $\geq 49$ copies after the last round of Cell-SELEX. Only the random region is presented .....	39
---	----

Table 3.2. Prediction of the folding of aptamer #1 and aptamer #2 at 37 °C and 4 °C. Only the structure(s) with the lowest free energy (dG) are presented. The loops are marked in the black rectangles .....	41
---	----

Table 3.3 Possible targets of aptamer #1 and aptamer #2 on MDA-MB-231 cell line .....	54
---	----



## LIST OF ABBREVIATIONS

5 – FU: 5-fluorouracil

ALPs: Anionic Liposomes

AR: Androgen Receptor

BL: Basal - Like

BSA: Bovine Serum Albumine

CL: Claudin - Low

CLPs: Cationic Liposomes

CSCs: Cancer Stem Cells

CT: Computed Tomography

DAPI: 4',6-diamidino-2-phenylindole

DLS: Dynamic Light Scattering

DMEM: Dulbecco's Modified Eagle Medium

DOX: Doxorubicin

D-PBS: Dulbecco's Phosphate-Buffered Saline

EDC: 1-ethyl-3-(3-dimethylaminopropyl)

EDTA: Ethylenediamine Tetraacetic Acid

EGF: Epidermal Growth Factor

EGFR: Epidermal Growth Factor Receptor

ER: Estrogen Receptor

FBS: Fetal Bovine Serum

FDG: 2-deoxy-2- [fluorine-18] fluoro-D-glucose

FDG – PET: Fluorodeoxyglucose-positron emission tomography

GNPs: Gold Nanoparticles

GSE-A: Gene Set Enrichment Analysis

HER2: Human Epidermal Growth Factor Receptor 2

IHC: Immunohistochemistry

IM: Immunomodulatory

iron oxide MNPs: Superparamagnetic Iron Oxide Nanoparticle

## LIST OF ABBREVIATIONS

$K_D$ : Dissociation Constant

LAR: Luminal Androgen Receptor

M: Mesenchymal

MSL: Mesenchymal stem-like

miRNA: MicroRNA

MNPs: Magnetic Nanoparticles

MRI: Magnetic Resonance Imaging

PARP: Poly ADP-ribose Polymerase

PBS: Phosphate-Buffered Saline

PCR: Polymerase Chain Reaction

PEG: Polyethylene Glycol

PET: Positron Emission Tomography

PFA: Paraformaldehyde

PR: Progesterone Receptor

PSMA: Prostate Specific Membrane Antigen

QDs: Quantum Dots

SDS-PAGE: Sodium Dodecyl Sulfate Polyacrylamide Gel Electrophoresis

SELEX: Systematic Evolution of Ligands by Exponential Enrichment

siRNA: Small Interfering RNA

SRB: Sulforhodamine B

SNPs: Silica Nanoparticles

Sulfo-NHS: N-Hydroxysulfosuccinimide Sodium Salt

TNBC: Triple Negative Breast Cancer

TAE: Tris-Acetate EDTA

## MOTIVATION AND AIM OF THE PROJECT

TNBC is a heterogenous disease with an aggressive and metastatic nature. Diagnosis is very important and decisive to ensure an early and appropriate therapeutic.

Aptamers are short single-stranded oligonucleotides (DNA or RNA) that can bind to target molecules with high affinity and specificity. Besides, they are able to be conjugated with nanomaterials.

In this project, previously selected aptamers for TNBC were validated through flow cytometry and fluorescent microscopy. Then, the dissociation constant of both aptamers was determined and their toxicity, as well as the silica nanoparticles toxicity *per se*, were evaluated using SRB assay. Two aptamers, aptamer #1 and aptamer #2, were conjugated with nanoparticles and these were further validated using a TNBC cell line. The possible targets for both aptamers were isolated. The main aim was to develop an aptamer-nanoparticle complex able to diagnostic TNBC in a earlier stage. For that purpose, there were specific aims along the project needed to be fulfilled. The nanoparticles were functionalized with the selected aptamers using the carbodiimide chemistry. Then, the functional nanoparticles were characterized and the efficiency of functionalization determined. Lastly the initial plan included the characterization of the affinity and selectivity of aptamer-nanoparticle conjugates through fluorescence microscopy and flow cytometry using different TNBC cell lines.

If successful, these aptamer-based diagnosis nanoparticles can be considered in the future for TNBC diagnosis.



# CHAPTER 1

## INTRODUCTION





Breast cancer is a heterogeneous and complex disease which incidence is increasing due to many factors such as lower age of menarche, late age of first pregnancy, fewer pregnancies, shorter or no periods of breastfeeding, and a later menopause (Howell et al., 2014). It is characterized by its distinct cellular origins, mutations, histology, evolution, potential to generate metastasis, response to therapy and clinical outcome (Mendes et al., 2015). Due to its heterogeneity, it is challenging to make an effective detection and diagnosis, as well as to resort to adequate therapy (Nobrega et al., 2016). Initially, detection and diagnosis were based on morphological observations. In the early 1900s, X-ray was first suggested for breast cancer detection. However, mammography only became an accepted technology in the 1960s, after technical innovations were introduced that produced higher-quality images that were more reproducible and easier to interpret (Nass et al., 2001). Immunopathological classification through high-throughput methods was the only one that has shown to be helpful to clinicians in the therapeutic decision-making process (Mendes et al., 2015). New and improved technologies are emerging and providing early detection.

High-throughput methods have allowed to identify the specific biomarkers' presence or absence enabling to distinguish different types of breast cancer (Mendes et al., 2015). The currently accepted biomarkers include the estrogen (ER), progesterone (PR) and human epidermal growth factor 2 (HER2) receptors, which presence or absence allow to identify four groups of breast cancer: ER<sup>+</sup>/PR<sup>+</sup>/HER2<sup>+</sup>, ER<sup>+</sup>/PR<sup>+</sup>/HER2<sup>-</sup>, ER<sup>-</sup>/PR<sup>+</sup>/HER2<sup>+</sup> and ER<sup>-</sup>, PR<sup>-</sup>, HER2<sup>-</sup>, or triple negative breast cancer (TNBC) (Mendes et al., 2015).

The breast cancer classification is a driver to set the adjuvant treatment approach for the disease at an early stage. HER2<sup>+</sup> cancers are treated with HER2<sup>+</sup> targeted therapy. This therapy involves the use of anti-HER2 antibodies (Hirshfield & Ganesan, 2014). Due to the absence of expression of recognizable sites for therapy, some breast cancers lack targeted options (Nobrega et al., 2016).

### 1.1 Triple Negative Breast Cancers (TNBC)

TNBC are tumours that lack the expression of both ER and PR, as well as lack the over-expression and/or lack the gene amplification of HER2 (Mayer, et al., 2014; Stockmans et al., 2008). Through gene expression analysis, TNBC can be identified by the mRNA levels' profiles of ER, PR and HER2 (Mayer et al., 2014).

TNBC accounts approximately 15% of all breast cancers newly diagnosed (Wu et al., 2017).

#### 1.1.1 TNBC Subtypes

TNBC is a heterogeneous disease that encompasses more than one type of tumour. Studies where Gene Set Enrichment Analysis (GSE-A) was performed indicated various subtypes of TNBC that were characterized based on gene ontologies and differential gene expression, as summarized in Table 1.1. One of those subtypes is the basal-like (BL) and exhibits low signals for ER and HER2, expresses proliferation genes and a unique cluster of basal genes, including basal cytokeratins and epidermal growth factor receptor (EGFR) (Dawood, 2010; Lehmann et al., 2011). BL1 tumours are BL tumours that are enriched in components of the cell cycle and division and pathways. BL1 subtype has a high proliferative nature, as well as a cell cycle checkpoint loss. As for BL2 subtype, besides its unique gene ontologies involving growth factor signalling, glycolysis and gluconeogenesis, it is enriched in EGFR and myoepithelial markers (Lehmann et al., 2011, 2016).

Immunomodulatory (IM) TNBC is composed by genes that encode immune antigens, cytokine and core immune signal transduction pathways. It is likely to represent gene expression from tumour cells and infiltrating lymphocytes. The IM signalling is evidenced by immune cell-surface antigens, complement cascade, antigen presentation, among others. Immune signalling genes overlap with the medullary breast cancer's gene signature. This is a histologically distinct form of TNBC (Lehmann et al., 2011, 2016).

Mesenchymal (M) subtype flaunts genes that are enriched in components and pathways involved in cell motility, extracellular matrix receptor interaction and cell differentiation pathways. Mesenchymal stem-like (MSL) shares gene enrichment similar to M subtype. However, genes that

represent components and processes involved in growth factor signalling pathways such as EGFR, G-protein coupled receptor are associated with MSL subtype (Lehmann et al., 2011).

Luminal androgen receptor (LAR) subtype expresses luminal gene and is enriched with pathways that are regulated by hormones as steroid synthesis, porphyrin metabolism, and androgen/estrogen metabolism. This subtype is although ER negative. LAR has a very high expression of androgen receptor (AR) mRNA and is associated with older patients (Lehmann et al., 2011, 2016).

Claudin-low (CL) subtype, besides being ER-, PR- and HER2-, presents a downregulation of claudin-3, claudinin-4 and claudinin-7, as well as low expression of marker Ki67, a protein associated with cell proliferation present in the active phases of cell cycle (Nobrega et al., 2016; Scholzen & Gerdes, 2000; Holliday & Speirs, 2011). CL subtype is also associated enrichment for markers associated with epithelial-mesenchymal transition and expression of features associated with mammary cancer stem cells (CSCs) (Holliday & Speirs, 2011).

Table 1.1. Summary of Triple negative breast cancer subtypes and its main characteristics

Subtype	Characteristics
Basal-like (BL) (Dawood, 2010)	Basal-like 1 (BL1) high cell cycle and DNA damage response gene expression; high Ki67 and cell cycle checkpoint loss (Lehmann et al., 2011; Nobrega et al., 2016; Scholzen & Gerdes, 2000)
	Basal-like 2 (BL2) enriched in growth factor receptor (EGFR), myoepithelial markers (highTP63 and MME)
Immunomodulatory (IM)	immune cell signalling, cytokine signalling, antigen processing and presentation, and signalling through core immune signal transduction pathways (Lehmann et al., 2011)
Mesenchymal stem-like (MSL) (Lehmann et al., 2011)	components and processes linked to growth factor signalling pathways cell motility, cellular differentiation, and growth pathways
Mesenchymal (M) (Lehmann et al., 2011; Holliday & Speirs, 2011)	Extracellular matrix receptor interaction
Luminal androgen receptor (LAR)	Luminal gene expression; driven by AR (Lehmann et al., 2011)
Claudin-low (CL)	Low Ki67, E-cadherin, claudin-3, claudinin-4 and claudinin-7 (Holliday & Speirs, 2011)

One of the first molecular discoveries about TNBC was that they are likely to arise in patients who carry the BRCA1 – a gene that plays role in double-stranded DNA's break repair-mutation and have gene expression profiles to tumours that are BRCA1-deficient. BRCA1-deficient tumours are sensitive to Poly ADP-ribose polymerase (PARP) inhibitors, once PARP enzymes are critical for appropriate processing and repair of DNA breaks (Lehmann et al., 2011).

In this project, the TNBC cell line MDA-MB-231 (Figure 1.1) which is a highly invasive ML cell line, was used (Lehmann et al., 2011)

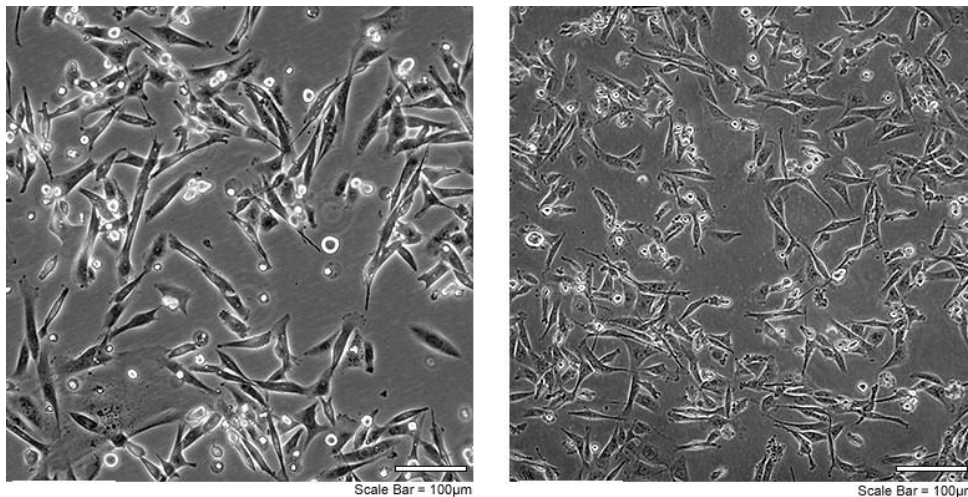


Figure 1.1. MDA-MB-231 cell line in low (left) and high (right) density. (from American Type Culture Collection)

### 1.1.2 TNBC Screening

Screening and diagnosis are very important and decisive to ensure an early and appropriate therapeutic, especially given the aggressive and metastatic nature of TNBC. Screening methods include radiological exams, such as mammography, ultrasonography, magnetic resonance imaging (MRI) and biopsy for lack of ER, PR and HER2 through immunohistochemistry (IHC) tests (Stockmans et al., 2008). However, TNBC in women that are over 50 years old are less likely to be detected through either mammography or ultrasound than women with non-TNBC (Dawood, 2010).

Several studies analysed the radiological characteristics of TNBC which include the presence of a smooth circumscribed mass, generally a lack of calcifications and/or spiculated margins on a mammogram, and a lack of an echogenic halo on ultrasound (Dawood, 2010; Stockmans et al., 2008). A retrospective look at MRI showed features associated with this type of breast cancer that include the presence of a mass lesion dominated by ductal phenotype with malignant enhancement kinetics, rim enhancement, persistent enhancement pattern and very high intratumoural signal intensity on T2-weighted MRI (Dawood, 2010).

Fluorodeoxyglucose-positron emission tomography (FDG-PET) combines the technique positron emission tomography (PET), an imaging method that constructs three-dimensional images by measuring radiolabelled tracer molecules, with 2-deoxy-2- [fluorine-18] fluoro-D-glucose (FDG), a tracer glucose analogue that is taken up by cells and allows to identify the regions where glucose uptake is increased (Dawood, 2010; Mendes et al., 2015; Stockmans et al., 2008). The increase of glucose uptake is a characteristic of tumour tissues, allowing the detection of metabolic alterations even before morphological changes occur (Mendes et al., 2015).

FDG-PET was used to compare the findings in TNBC with those in oestrogen receptor positive/progesterone receptor positive/HER2 negative tumours (Stockmans et al., 2008). Results showed a higher FDG uptake in TNBC (Dawood, 2010; Stockmans et al., 2008). The sensitivity for detection allows distinguishing different types of breast cancer (Stockmans et al., 2008).

Developments in the field of synthetic biology allowed to develop specific contrast agents with potential molecular imaging applications. Molecular imaging resorts molecular probes in order to detect key biological processes by coupling signal or contrast agents with ligands targeting upregulated or overexpressed receptors (Chinen et al., 2015; Mendes et al., 2015). This approach allows a molecular examination of tumours since they occur early in the disease. Antibodies, peptides and aptamers fall into this group of molecules that can be combined with signal agents (Mendes et al., 2015).

Antibodies are the most studied class of targeting ligands and their introduction revolutionized the management of TNBC (Dawood, 2010; Mendes et al., 2015). Antibodies are single protein molecules that contain two epitope binding sites which provide high selectivity and

affinity for binding targets. Nowadays, engineering allows its production with capability of recognising the desired molecule or with other desired features. Imaging probes can be attached to antibodies in order to perform exams however, these molecules are expensive and conjugation with signalling agents can be problematic (Mendes et al., 2015).

Peptide ligands that specifically recognize cell-surface receptors are a promising class of low weight ligands (Mendes et al., 2015). They present high specificity and affinity for target binding, low immunogenicity and reduced production costs. Therefore, peptides have been extensively used in cancer research (Mendes et al., 2015; Nobrega et al., 2016; Silva et al., 2016). When associated with signalling agents, peptide's biodistribution may be negatively affected (Mendes et al., 2015). In order to discover new target binding peptides evolutionary screening techniques, such as Phage Display, have emerged as a powerful tool (Mendes et al., 2015). Using the Phage Display technique, peptide libraries are screened against a receptor or a group of receptors to select peptides that exhibit binding capacity towards the desired receptors (Mendes et al., 2015; Silva et al., 2016). Specific and selective peptides for the MDA-MB-231 cell line have already been retrieved using this technique (Nobrega et al., 2016).

Aptamers are short single stranded nucleic acids (DNA and RNA) that fold into three-dimensional structures and are capable of binding to targets with high specificity and affinity (Mendes et al., 2015; Prakash & Rajamanickam, 2015). Similar to peptides and antibodies, aptamers can be combined with signalling agents to enable tumours visualization (Prakash & Rajamanickam, 2015). Aptamers will be further discussed in the following subsections.

### 1.1.3 TNBC Treatments

Nowadays, breast cancer therapy is selected for each patient according to the presence of ER, PR and HER2 biomarkers. However, as previously mentioned, patients with TNBC do not express these receptors, which narrows the available treatments. Treatment options include surgery, radiotherapy and classical chemotherapy (Silva et al., 2016). Nanotechnology-based drug delivery systems containing encapsulated, dispersed, absorbed or conjugated drugs can lead to enhanced performance. Nanoparticles can have higher saturation, rapid dissolution and enhanced

adhesion to biological surfaces (Mendes et al., 2015; Prakash & Rajamanickam, 2015). Combining target binding molecules, such as antibodies, peptides and aptamers, would possibly reduce the drug dose needed to achieve a therapeutic benefit, lowering the side effects (Prakash & Rajamanickam, 2015).

The administration of therapeutic agents directly in the tumour can reduce the effect loss, as well as the dose needed to attain the same effect. However, it requires constant intratumoral injections. It is common to administer a combination of cytotoxic compounds to patients that include anthracyclines (antitumour antibiotics that interfere with the enzymes involved in the DNA replication) and taxanes (that damage cells in all cell cycle phases; indeed they act by stopping the mitosis or inhibiting the synthesis of proteins involved in cell reproduction). Capecitabine (prodrug of 5-fluorouracil (5-FU) that belongs to the anti-metabolites class of drugs) is administered at the time of the progression. Unfortunately, the limited treatment options and potential resistance to these cytotoxic agents demand the development and use of alternative chemotherapeutic agents. Eribulin and ixabepilone are non-taxane mitotic inhibitors used in the therapy of metastatic TNBC (Crown et al., 2012). Approved agents for breast cancer therapy have a poor prognosis for these patients.

Hyperthermia-mediated drug delivery is one of the potential treatments for TNBC. In summary, an heat-activated thermosensitive liposome is administered to the cells by a laser set-up until reaching 42 °C, leading to a reinforcement of the effect of administered drugs (Dunne et al., 2018).

To avoid repeated injections, a nanofluidic-based device for intratumoral drug delivery called the nanofluidic drug-eluting seed was developed (Chua et al., 2018). The device loaded with monoclonal antibodies against TNBC attained great anti-tumour response, as well as a sustained drug concentration in the tumour and microenvironment with minimal systemic exposure.

## 1.2 Aptamers

Cell surface receptors are usually differentially expressed in cancer cells as compared to normal cells (Meng et al., 2015; Prakash & Rajamanickam, 2015). Therefore, exploring the

presence, over or under expression of certain cell surface receptors allows developing early detection solutions (Prakash & Rajamanickam, 2015).

Aptamers are short (10- 100 nucleotides), single-stranded oligonucleotides (DNA or RNA) with the ability to form tertiary structures (Ku et al., 2015; Liu et al., 2014). These molecules can bind to various molecular targets with high affinity and specificity (Prakash & Rajamanickam, 2015). Aptamers are cheaper than other molecules, exhibit low immunogenicity and toxicity, are small enough to penetrate into solid tumours and able to reversibly denaturate and refold without losing activity (Liu et al., 2014; Ma et al., 2015). Aptamers have increased its usage as a biotechnological tool for validation and interaction with proteins and ligands, as well as its use as a characterization tool to interact with a molecular pathway (Prakash & Rajamanickam, 2015). This last usage allows studying the biochemical nature of the disease, which could give some idea about its progression pattern (Prakash & Rajamanickam, 2015). Aptamers are excellent candidates as molecular probes for diagnosis and treatment of cancer, being able to be conjugated with nanomaterials (Hong-min Meng et al., 2015).

These molecules can be identified through an *in vitro* iterative process “Systematic evolution of ligands by exponential enrichment” (SELEX) that includes multiple rounds of selection, amplification and washing (Liu et al., 2014). SELEX (Figure 1.2) allows the isolation of functional nucleotide sequences from a DNA or RNA library in which may exist a sequence or a set of sequences capable of performing aptamer-target recognition (Ku et al., 2015). This recognition occurs through intermolecular interactions such as aromatic rings, pi-pi system stacking, van der Waals and electrostatic interactions between charged groups and hydrogen bonding (Ku et al., 2015). In order to bind to a target, aptamers may have to undergo adaptive conformational changes, including having their three-dimensional structure folded into a unique binding conformation (Ku et al., 2015; Ma et al., 2015).



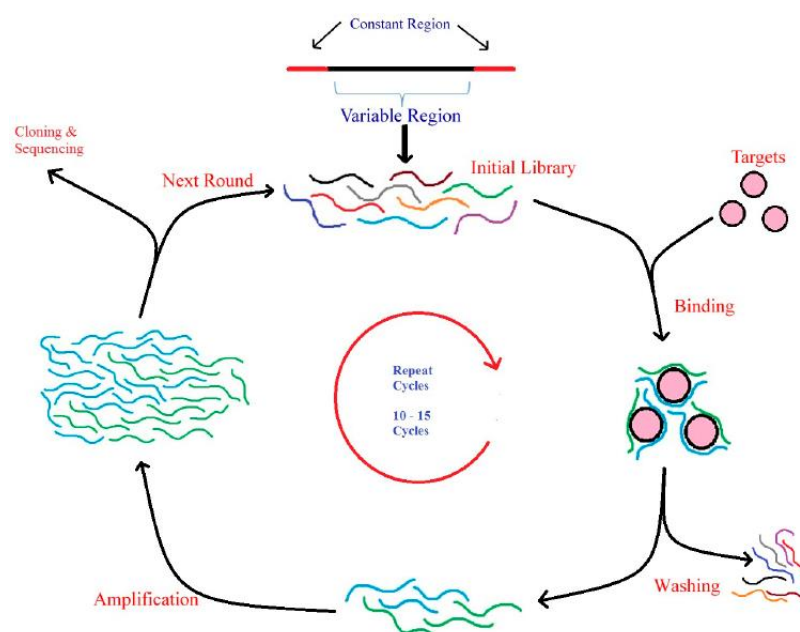


Figure 1.2. Schematic representation of the SELEX process (Prakash & Rajamanickam, 2015).

The SELEX process starts with the synthesis of a pool of oligonucleotide sequences – a library (Ku et al., 2015). Each sequence has two constant sequences that work as primer binding sites for polymerase chain reaction (PCR) amplification and a central random sequence (Ku et al., 2015). Then, the oligomers are incubated with the target molecule or target cell, to which some will bind (Prakash & Rajamanickam, 2015). After this step, the oligonucleotides are eluted and the ones that bound to the target are amplified, creating a new pool of sequences that will be used in the following round (Ku et al., 2015; Prakash & Rajamanickam, 2015). This process is repeated until high-specificity aptamers are attained (Prakash & Rajamanickam, 2015).

The cell surface is complex and has many different molecules that play crucial roles in the cells behavior and activity (Ku et al., 2015; Hong-min Meng et al., 2015). Using Cell-SELEX it is possible to identify aptamers that bind to a certain cell type based on the cell's extracellular characteristics, requiring no prior information about cell surface biomarkers (Ku et al., 2015). Cell-SELEX has been extensively used in cancer research and allowed to find specific sequences that can be used as probes for early cancer detection or cancer-related biomarkers, as well as targeted delivery of therapeutics into cancer cells (Ku et al., 2015; Hong-min Meng et al., 2015). Through this process, 8 to 20 rounds of selection may be performed using both cancer cells and healthy

cells to retrieve the most specific sequences (healthy cells are used in counter-selection rounds) (Ma et al., 2015).

As SELEX, Cell-SELEX begins with the design of a library of fluorescence-labeled sequences and primers that will allow to amplify the sequences through PCR. This is followed by the selection that demands a negative selection with healthy cells. Selection also requires live cells as target in either an adherent monolayer or dissociated cells. The sequences are recovered by heating the cell-aptamer complex, since aptamers can denaturate and refold without losing activity, and the ssDNA pool is eluted and used in the next round of selection (Ma et al., 2015; Hong-min Meng et al., 2015). PCR is very important in this process and is applied between selection rounds. Selection is only completed when no significant difference between the fluorescence signal intensity of the control background and the selected DNA pools is observed, and when no significant signal difference can be found between successive selected pools (Ma et al., 2015).

### 1.2.1 Aptamers in cancer diagnosis

Aptamers are able to specifically recognize almost any oncoprotein, cancer metabolite and cancer cell, thus making them an interesting tool when it comes to cancer diagnostic (Liu et al., 2014). Aptamers, as target recognition moieties, have been coupled to various transduction platforms to demonstrate their applicability for biosensing, being used in optical assays, electrochemical assays and mass difference assays (Ma et al., 2015). For this purpose, aptamers are used as the recognition element in the development of novel biosensors (Prakash & Rajamanickam, 2015).

Molecular imaging techniques enable visualizing the tumour, as well as tracing and measuring the expression and activity of the molecules that influence its behavior and response to therapy (Ma et al., 2015). Aptamers do not have optical properties. Thus, in order to be useful in optical molecular imaging assays, aptamers need fluorescent dyes that can be conjugated with either its 5' or 3' end and, for *in vivo*, this aptamer-conjugated can circulate until binding the target cell or tissue (Ku et al., 2015). Anti-EGFR aptamers conjugated with dyes have been used to determine the expression of normal EGFR and mutated EGFR (Li et al., 2010).

Aptamer-conjugated magnetic nanoparticles (MNPs) have been used for MRI and have been shown to be taken up by cancer cells. This complex can be detected with very few cancer cells, because most biological samples exhibit no magnetic background (Opazo et al., 2012). Aptamer-conjugated MNPs are able to accommodate multiple aptamer-binding events. To create a cellular molecular profile, an array of aptamer-conjugated MNPs has been used allowing clinicians to identify cancer cells more accurately (Bamrungsap et al., 2012). Aptamer-quantum dots (aptamer-QDs) have been conjugated with anti-prostate specific membrane antigen (PSMA) aptamer and superparamagnetic iron oxide nanoparticles (iron oxide MNPs) for prostate cancer imaging, therapy and monitoring of the drug. This complex is used for optical imaging or MRI. Different QDs can be used in association with different aptamers as these contrast agents can have distinct emission wavelengths (Bagalkot et al., 2007). The MNPs usage will be further discussed.

Many aptamer conjugates are targeted to bind on the surface of a specific type of cancer cell through the specific recognition of the target on the cell membrane surface by its aptamer. Gold nanoparticles (GNPs) possess distance-dependent optical properties, changing colour. Using PSMA binding aptamer conjugated with GNPs it is possible to visualize prostate cancer via electrochemical assays such as Computed Tomography (CT) (Kim et al., 2010). AS1411 conjugated with  $^{64}\text{Cu}$  allows to visualize early lung cancers (J. Li et al., 2014).

Ultrasound imaging is the most common clinical imaging modality, although limited by image resolution (Prakash & Rajamanickam, 2015). To overcome this limitation, contrast agents, such as microbubbles, have been developed and conjugated with aptamers, formulating molecular ultrasound probes. Microbubbles are designed to show, for example, ultrasound activation when thrombin levels are associated with clot formation. Therefore, microbubbles are coated with aptamers and DNA, binding to the target and causing the removal of the aptamer from the microbubble-polymer DNA complex (Nakatsuka et al., 2012). This removal causes the generation of ultrasound signals.

Nuclear imaging has the highest potential for clinical translation of aptamer-conjugated molecular probes. Radiolabeled TTA1, an aptamer targeted against extracellular matrix protein tenascin-C, was used in breast cancer (MDA-MB-435 cell line) and showed rapid blood clearance

from renal and hepatic pathways, as well as a fast but durable tumour penetration (Pieve et al., 2009). Aptamer LXL-1 was selected through cell – SELEX with the aim of detecting metastatic breast cancer, combining this aptamer with molecular probes. It was shown that the truncated version of this aptamer, LXL-1-A, had high affinity for metastatic breast cancer, as well as selectivity (Li et al., 2014).

### 1.2.2 Aptamers in cancer treatment

Conventional cancer therapies such as chemotherapy, radiotherapy and photothermal therapy affect both cancer cells and healthy cells. Targeted therapy has been designed to avoid side effects and increase efficiency and it first started with the use of antibody-based drugs (Prakash & Rajamanickam, 2015). However, antibodies are expensive molecules that cannot be obtained by chemical synthesis. Aptamers present, as seen above, low immunogenicity, high stability, and are easy to produce and modify (Mendes et al., 2015). Moreover, as previously mentioned, aptamers can be conjugated with nanoparticles and nucleic acids for efficient targeted treatments (Prakash & Rajamanickam, 2015).

Aptamers can be conjugated with gene silencing tools, such as small interfering RNA (siRNA) and microRNA (miRNA), being used as guiding molecules for precise delivery to increase target specificity of these nucleic acid moieties (Prakash & Rajamanickam, 2015).

Anti-PSMA aptamer was conjugated to anti-lamin A/C siRNA, resulting in a aptamer-mediated siRNA delivery to the prostate tumour cells that express PSMA on their surface (Chu et al., 2006). In response to this therapy, gene expression was inhibited. In other cases, aptamer-siRNA chimeras were generated for siRNA target delivery (McNamara et al., 2006). These aptamers could, just like the previous ones, bind to PSMA expressing cells and were bound to two different siRNAs. The siRNAs target different genes, leading to their silencing and hindering the *in vivo* tumour growth (Prakash & Rajamanickam, 2015). It is also possible to resort to different aptamers for the same target bound to siRNA, forming a bivalent aptamer-siRNA chimera. This bivalent chimera presents prolonged half-life and enhanced *in vivo* tumour inhibition when compared to monovalent chimera (Wullner et al., 2008).

miRNA can be used for targeted cancer therapy with the junction of appropriate aptamers (Ma et al., 2015; Prakash & Rajamanickam, 2015). A complex consisting of an aptamer towards MUC1 and miRNA was designed to target ovarian carcinoma cells. This complex has shown to be internalized and, as result of its action, DNA methyltransferase gene expression was downregulated (Esposito et al., 2014).

Liposomes are the most successful drug-delivery systems that have been approved (Ku et al., 2015). Aptamers can be spontaneously anchored to these nanoparticles, improving the specificity and efficacy of the treatment (Ku et al., 2015; Liu et al., 2014). Aptamers against E-selection were conjugated with liposomes and were intravenously administered. As a result, the complex accumulated at the vasculature of the breast tumour with no circulation half-life shortening (Mann et al., 2011).

As seen previously, GNPs can be conjugated with aptamers in order to diagnose cancer. However, this complex can also be applied to cancer therapy when the GNPs are loaded, for example, with doxorubicin (DOX). Anti-PSMA aptamers conjugated with GNPs loaded with DOX has shown to be very efficient killing of prostate cancer cells (Kim et al., 2010).

Although GNPs can be loaded with drugs to treat cancer, these nanoparticles, as well as MNPs have been tested also for targeted cancer thermotherapy. In this type of therapy, cancer cells are destroyed by excessive heat, turning these nanoparticles into photothermal nanotherapy drugs (Kuo et al., 2010). GNPs present a strong absorption in the near-infrared light spectrum, serving as highly efficient energy quenchers and hyperthermia agents for photothermal therapy.

QDs, similarly to GNPs, can simultaneously be used as diagnostic and therapy aptamer conjugates. A pH-responsive QD-mucin1 aptamer-doxorubicin for ovarian cancer chemotherapy was developed (Savla et al., 2011). QDs were conjugated with an aptamer specific for mutated mucin1 that is overexpressed in ovarian cancer cells and in other cancer cells. DOX was attached to quantum dots via a pH-sensitive bond, which provided stability for systemic circulation and drug release inside target cells (Savla et al., 2011). The results showed the stability in neutral and slightly basic pH and the fast hydrolysis in acidic pH, allowing the complex to be applied *in vivo*.

MNPs are useful for cancer diagnosis and therapy. These can be modified by the conjugation of targeting ligands and drugs to provide multimodal functionality (Zheng et al., 2013). These particles have been loaded with a photodynamic therapy agent and conjugated with the AS1411 aptamer – used to target myeloid leukemia and renal cell carcinoma. This complex promoted targeted delivery, increased accumulation at the target site and prevent toxicity in neighbour tissues.

Recently, an aptamer guided liposome loaded with a siRNA was built as an attempt to treat metastatic breast cancer resorting to previously described aptamer LXL-1-A (Alshaer et al., 2018). The nanocarrier was tested *in vitro*, as well as *in vivo* and in both cases, the siRNA-loaded liposome bound successfully to the target in the membrane and also silenced the reporter gene luciferase. Such nanocarrier shows that it is possible to silence genes in metastatic breast cancer, in the perspective of silencing disease-related genes in tumours.

Aptamers can be used in cancer therapy as a directing molecule for drug delivery. However, aptamers can bind to a target and block or modulate the biological activities of target proteins (Zhu et al., 2012). Anti-EGFR aptamers can intercept receptor tyrosine kinase signal pathway, blocking EGFR autophosphorylation by binding to this receptor. This will affect the treated cells' ability to migrate (Wan et al., 2014). Aptamers remain an unpredictable class of therapeutics due to the limited prevalence of published information.

Although these therapies may allow the patient to experience less side effects whilst being effective against the tumour cells, many of these targeted therapies that use aptamers are not conventionally applied outside the research field and only a few of them are currently in clinical trials, which is the case of AS 1411 and NOX- A12 (Camorani et al., 2018; Wu et al., 2017).

Currently, Macugen (commercial name for the aptamer Pegaptanib) is the only aptamer based treatment approved by Food and Drug Administration and European Medicines Agency. It is directed for eye diseases such as proliferative diabetic retinopathy, diabetic macular oedema and age-related macular degeneration (Wu et al., 2017; Zhou & Rossi, 2017).

### 1.3 Nanoparticles

Effective treatment against TNBC requires an integrated therapeutic approach that addresses critical issues in cancer therapy. Nowadays, there is no biomarker that ensures that therapy will be successful. There are two major challenges in the management of TNBC patients namely monitoring the therapeutic response and effective treatment of drug resistant tumours (Miller-Kleinhenz et al., 2015). The development of targeted diagnostic and therapy nanoparticles provides a platform for drug loading, as imaging agents or therapy agents themselves (Ku et al., 2015). As previously mentioned, these nanoparticles are often associated with molecules that bind specifically to a target, being aptamers one of those molecules. Many of the existing nanoparticles for cancer diagnosis and treatment are, however, not yet used in clinical practice.

Some of the nanoparticles with potential to be used have already been mentioned. Liposomes, MNPs and aptamers are some of the nanoparticles with potential to diagnose and/or treat cancer and TNBC.

#### 1.3.1 Liposomes

Liposomes were the first nanoparticle drug carriers developed and consist of single or multiple concentric lipid bilayers that encapsulate an aqueous compartment (Bozzuto & Molinari, 2015; Miller-Kleinhenz et al., 2015). Notable progress has been made, and several biomedical applications of liposomes are either in clinical trials or are about to be put on the market, while others have already been approved for public use (Bozzuto & Molinari, 2015). Liposomes are capable of reducing side effects of chemotherapeutic drugs, that are quite toxic to cancer and normal cells, whilst enhancing their efficacy (Yingchoncharoen et al., 2016). Besides their efficiency, liposomes are biocompatible and biodegradable and have a structure that gives them the ability to contain both hydrophilic and hydrophobic drugs (Bozzuto & Molinari, 2015). Liposomes coated with polyethylene glycol (PEG) decrease nonspecific uptake by macrophages, increasing their half-life in the blood and bioavailability to tumours (Miller-Kleinhenz et al., 2015). The PEG liposome loaded with arsenic oxide resulted in increased accumulation in tumours and

enhanced antitumour effect when compared to free arsenic oxide in MDA-MB-231 cell line (Miller-Kleinhenz et al., 2015).

Physical properties such as size and surface charge are important. Size influences clearance, being shown that bigger liposomes (>200 nm) exhibit a faster rate of intravascular clearance via splenic filtration and hepatic sequestration (Yingchoncharoen et al., 2016). This property also influences uptake by organs and tissues (Yingchoncharoen et al., 2016).

Cationic liposomes (CLPs) consist of natural neutral phospholipids and positively charged lipids (Bozzuto & Molinari, 2015). Positive charge enhances the transfection of anionic animal target cells, and make these particles able to cross the blood–brain barrier (Bozzuto & Molinari, 2015). Anionic liposomes (ALPs) are prepared from negatively charged phospholipids and are less stable than CLPs, suffering opsonization when injected in the blood circulation (Bozzuto & Molinari, 2015; Yingchoncharoen et al., 2016). It is thought that both normal and cancer cells respond to these liposomes in the same way (Yingchoncharoen et al., 2016).

### 1.3.2 Magnetic nanoparticles

Magnetic materials show response to an applied magnetic field (Issa, Obaidat, Albiss, & Haik, 2013). MNPs have been extensively studied for biomedical applications such as MRI contrast agents, iron deficiency treatment, thermal and magnetic targeting therapy and drug delivery due to biocompatibility and supermagnetic properties (Hauser et al., 2015; Yallapu et al., 2011). To extend circulation time in the biological environment, MNPs provide means for functionalization with targeting agents or fluorescent markers or afford the opportunity for drug loading and conjugation, being often coated with or embedded in a polymer or organic matrix (Hauser et al., 2015).

MNPs have biomedical applications, as mentioned before, and have the ability for simultaneous diagnosis and therapy in a single formulation (Yallapu et al., 2011). The usage of MNPs in MRI presents advantages such as enhancing the image contrast between the normal and diseased tissue and indicate the status of organ functions or blood flow (Akbarzadeh et al., 2012). To detect cancer metastasis it is possible to use MNPs, such as iron oxides, as contrast agents in



MRI. The first element to be used for this purpose was manganese that rapidly was replaced by gadolinium, as the last one has relatively large magnetic moment due to the seven unpaired electrons. Nowadays, these elements have been replaced by ferromagnetic particles, mainly iron oxides, or ferrites (Issa et al., 2013).

These nanoparticles can also be applied in cancer therapeutics. Thermal therapy and drug delivery are two forms of therapy in which MNPs are used. MNPs can be synthesized in various sizes and be functionalized in order to carry various molecules (Gobbo et al., 2015). For therapy with drug delivery, MNPs need to be coated with organic polymers and inorganic metals or oxides to make them biocompatible and suitable for further functionalization by attaching various bioactive molecules (Akbarzadeh et al., 2012). Chemotherapeutics drugs like DOX have shown good results (Gobbo et al., 2015). Besides conjugation with targeting molecules, MNPs can be directed by a magnetized field that guide them to the target (Akbarzadeh et al., 2012).

Thermal therapy is focal and repeatable (Gobbo et al., 2015). MNPs can induce localized hyperthermia in an alternating magnetic field to potentially destroy cancer cells (Yallapu et al., 2011). In order to perform this treatment, MNPs need to be in the tumour environment, which is achieved via targeting (Hauser et al., 2015). The temperature rise occurs as a result of energy absorption from the applied magnetic field which is transferred from the MNPs as heat during reversal magnetization (Yallapu et al., 2011).

Superparamagnetic iron oxide MNPs have demonstrated to be suitable for diagnostic and therapy of cancer due to their intrinsic magnetic properties useful for MRI application and because of their easily modifiable surface by targetings ligands, dyes and drugs (Hong-min Meng et al., 2015). Iron oxide MNPs can be obtained through different methods and can address the challenges of tumour heterogeneity and adaptive resistance which can ultimately help to achieve the goal of personalized medicine for cancer therapy (Yallapu et al., 2011). The fine-tuning of the magnetic properties of the iron oxide MNPs can lead to change the relaxation rate of water protons in the immediate surroundings (Gobbo et al., 2015). A change of contrast and coating of the MNP is exhibited and side effects might be reduced, when applied in cancer therapy (Gobbo et al., 2015). Less amounts of iron oxide MNPs are needed to perform diagnosis in the patients, even when

compared to other MNPs, as iron oxide MNPs have an enhanced proton relaxation (Akbarzadeh et al., 2012). Coating is very important as it modifies cell interaction process, pharmacokinetics and biodistribution (Gobbo et al., 2015; Issa et al., 2013). Iron oxide MNPs can be conjugated with aptamers for targeted diagnosis and therapy. Anti-PSMA conjugated iron oxide MNPs loaded with DOX is an example of prostate cancer detection and simultaneous treatment (Hong-min Meng et al., 2015). Due to their supermagnetic nature, iron oxide MNPs can also be employed for hyperthermia therapy because of their fewer side effects (Yallapu et al., 2011).

### 1.3.3 Silica Nanoparticles

Silica nanoparticles (SiNPs), among other nanoparticles, have attracted attention due to their physicochemical properties (Song et al., 2017). Like MNPs, SiNPs' particle size is controllable, which influences their uptake, they are stable and biocompatible, present high loading capacity and are non toxic (Arap et al., 2013; Song et al., 2017; Z. Wang et al., 2016). SiNPs are a robust system used for the delivery of hydrophobic anticancer drugs (Z. Wang et al., 2016). Generally, these particles have negative charge (Arap et al., 2013). PEG, amine, carboxyl, and phosphate groups could be easily conjugated to change this charge and the binding to tumour site, affecting imaging and drug delivery (Bazak et al., 2016). SiNPs can be coated with polyelectrolyte layers, to prevent early leakage, functionalized by aptamers and loaded with anticancer drugs allowing controllable drug release under the appropriate conditions (Liu et al., 2014).

Luminescence measurements with luminescent SiNPs are very sensitive and offer great spatial resolution, presenting low detection limits, permitting the track down of biological events, highlighting the origin and growth of cancer. Optical imaging is easier to use and more cost-effective, when compared to MRI. Although SiNPs are photophysically inert, they may contain active species that increase the brightness and the signal (Arap et al., 2013).

These particles can be used both targeted and non-targeted (Arap et al., 2013). However, targeted SiNPs bind more successfully to the tumour cells, due to increased affinity and, in drug delivery systems, are more efficient in promoting cell death (Arap et al., 2013).

Several drugs can be loaded into SiNPs. DOX is used for treatment of cancer via delivery through SiNPs. pH can also be used as a triggering factor for drug release from SiNPs, by coating the nanoparticles with nanovalves responsive to the endosomal acidification conditions in cancer cells (Huan Meng et al., 2010).

Besides chemotherapy, SiNPs can be used in photothermal therapy, by loading photothermal agents, such as gold nanorods, in the nanoparticles and using a power density laser (Puvanakrishnan et al., 2012). As a result, the tumours cells are eliminated.



CHAPTER 2  
MATERIALS AND METHODS



Aptamers were previously selected and counter-selected using MDA-MB-231 and MCF-10-2A, respectively.

To select the aptamer sequences, 10 rounds of Cell-SELEX were performed, followed by counter-selection to prevent unwanted selectivity to non-tumorigenic cells. From this procedure 10 aptamers were chosen based on the number of copies, i. e., aptamers that had at least 50 copies in the entire sequenced pool. Out of the 10 aptamers fitting this request, 2 were synthesized for validation with the cell lines used for selection.

### Cell lines

In this work, two different cell lines were used, namely MDA-MB-231 (ATCC<sup>®</sup> HTB-26) and MCF-10-2A (ATCC<sup>®</sup> CRL-10781). MDA-MB-231 is a TNBC (i.e. it does not express ER, PR and HER2) with low expression of the proliferation marker Ki67, enrichment for markers associated with the epithelial-mesenchymal transition and expression of features associated with mammary cancer stem cells. This cell line was established in 1973, from the adenocarcinoma of a 51 years old adult Caucasian female, who was submitted to a mastectomy (Cailleau, Young, Olivé, & Reeves, 1974). It was isolated through pleural effusion from mammary gland/breast tissue and derived from metastatic site. This cell line was cultivated in DMEM supplemented with 10% (v/v) FBS and 1% (v/v) Zell Shield (Minerva Biolabs).

The control normal breast cell line MCF-10-2A was also used. This is an epithelial cell line obtained from breast mammary gland and was isolated from a 36 years old female diagnosed with fibrocystic disease (Soule et al., 1990). This cell line was cultured in DMEM: Ham's F12 media mixture (Merck) in 1:1 proportion supplemented with 5% (v/v) Horse Serum (Merck), 1% (v/v) Zell Shield, 0.1 % (v/v) Human recombinant insulin (Sigma), 0.05% (v/v) Hydrocortisone (Sigma), 0.02% (v/v) epidermal growth factor (EGF, Merck) and 0.01% (v/v) cholera toxin (Sigma).

The sterile manipulation of cells was performed in Mars Scanlaf (Labogene) Biological Safety Cabinets Class 2 and incubated in Heracell (Thermo Scientific) incubator at 5% (v/v) CO<sub>2</sub> and 37 °C.

When cells reached about 70 % to 90 % confluence they were subcultured. Firstly, the medium was removed and the cells were washed with 1 mL of pre warmed PBS 1X (137 mM NaCl, 2.7 mM of KCl (ChemLab), 10 mM of Na<sub>2</sub>HPO<sub>4</sub> (VWR) and 1.8 mM of KH<sub>2</sub>PO<sub>4</sub> (PanReac) dissolved in deionized water. The pH was adjusted to 7.4 using 1 M HCl (Fisher Scientific)). Then, 1 mL of 0.05% trypsin/0.2 mM EDTA was applied and the cells were incubated in Heracell incubator at 5% (v/v) CO<sub>2</sub> and 37 °C for about 5 min. To inactivate trypsin, 3 mL of complete medium was applied. About  $\frac{1}{4}$  of the cells were transferred to a new T75 and the necessary volume of medium to make up 7 mL was added.

## 2.1 Folding prediction

Using the free online application DNA fold from The Mfold Web Server (<http://unafold.rna.albany.edu/?q=mfold>), the folding structure of aptamer #1 and aptamer #2 was predicted. After the insertion of each sequence, the tool calculated the Gibbs free energy of each secondary structures, presenting the optimal and suboptimal structures for each aptamer at 4 °C and 37 °C.

The salt conditions used by default to predict the *in silico* conformation of the sequences were 74.3 mM Na<sup>+</sup> and 0.0233 mM Mg<sup>2+</sup>, which correspond to the salt concentrations from the Phosphate-buffered saline (PBS) 1X (Mg<sup>2+</sup>/Ca<sup>2+</sup>) used in the selection process.

## 2.2 *In vitro* studies

For the cell recognition experiments, the previously mentioned cell lines were cultured in the day before the experiment in a 6-well plate. For the fluorescence microscopy 3×10<sup>5</sup> cells per well were seeded. For flow cytometry about 0.5×10<sup>5</sup> cells per well were seeded.

Before performing the *in vitro* cell binding assays, the aptamers were boiled at 95°C for 5 min and then cooled for 10 min at room temperature. After these steps, the aptamers were ready for the experiments.



### Fluorescence Microscopy

The cell lines were cultured over glass slides in a 6-well plate.

On the day of the experiment, the culture medium was removed and the cells were washed two times with 500  $\mu$ L of pre-warmed PBS 1X. Next, 500  $\mu$ L of pre-warmed paraformaldehyde (PFA) were added to each well and incubated at room temperature for 40 min. The PFA was removed after the incubation and the wells were washed with 500  $\mu$ L of pre-warmed PBS 1X and the slides were transferred to a 24-well plate. After this step, 100  $\mu$ L of a solution of 250 nM of aptamer in PBS 1X supplemented with  $\text{Ca}^{2+}$  and  $\text{Mg}^{2+}$  (1 mM of  $\text{CaCl}_2 \cdot 2\text{H}_2\text{O}$  (Panreac) and 0.5 mM of  $\text{MgCl}_2 \cdot 6\text{H}_2\text{O}$  (VWR) was incubated in each slide for 30 min at 37 °C or at 4 °C. The aptamer solution was removed and the slides were washed two times with 100  $\mu$ L of pre-warmed PBS 1X. Then, 100  $\mu$ L of 4',6-diamidino-2-phenylindole (DAPI, Biotium) was added to each slide and incubated for 30 min at room temperature. The coverslips were placed in slides and the cells were observed in a fluorescence microscope (OLYMPUS BX51).

### Flow Cytometry

The cell lines were cultured in a 12-well plate.

On the day of the experiment, the culture medium was removed and the cells were washed two times with 500  $\mu$ L of pre warmed PBS 1X. After this step, 200  $\mu$ L of a solution of 250 nM of aptamer in PBS 1X supplemented with  $\text{Ca}^{2+}$  and  $\text{Mg}^{2+}$  was incubated in each well for 30 min at 37 °C or at 4 °C, instead. The aptamer solution was removed and the cells were washed two times with 400  $\mu$ L of pre warmed PBS 1X. With the help of cell scraper (SPL LifeSciences) the cells were detached and transferred into centrifuge microtubes.

The assay was performed at 4 °C and 37 °C once aptamers selected at 37 °C tend to internalize the target cells. Therefore, it was important to understand if the target was in the cell membrane.

### Membrane pre-treatment

Before the incubation of the aptamer, the cells were subjected to treatment with a 0.1 mg mL<sup>-1</sup> Proteinase K (Fisher BioReagents) solution for 3 or 10 min. A treatment with trypsin acid was also performed. In this case, the cells were incubated with 0.05% trypsin/0.2 mM Ethylenediamine tetraacetic (EDTA, Biochrom) for 3 min or 10 min. In both cases, the incubation occurred at 37 °C and the reaction was stopped by adding 100 µL of Dulbecco's Modified Eagle Medium (DMEM, Merck) with 10% (v/v) of Fetal Bovine Serum (FBS, Merck).

#### 2.2.1 Determination of the Dissociation Constant ( $K_D$ )

The dissociation constant ( $K_D$ ) was determined using flow cytometry.

On the day of the experiment, the culture medium was removed and the cells were washed two times with 1 mL of pre-warmed PBS 1X. After this step, 1 mL of a solution of aptamer (concentrations ranging from 0 nM to 400 nM) in PBS 1X supplemented with Ca<sup>2+</sup> and Mg<sup>2+</sup> was incubated in each well for 30 min at 37 °C. The aptamer solution was removed, the cells were washed two times with 1 mL of pre-warmed PBS 1X and, with the help of cell scraper, the cells were detached and transferred into centrifuge microtubes. The cell suspension was centrifuged at 220 g and resuspended in 200 µL of PBS 1X.

The aptamers  $K_D$  was calculated using the equation  $Y = B_{\max} X / (K_D + X)$ , where:

Y - % of fluorescent cells

$B_{\max}$  – slop maximum

$K_D$  – dissociation constant

X – concentration of aptamer, through GraphPad Prism 7.

#### 2.2.2 Cytotoxicity

##### Toxicity assay

Although the aptamer-nanoparticles conjugates are only meant to be used as a diagnostic method for TNBC, these conjugates can have negative effects in both cancer and normal cells. Therefore, Sulforhodamine B (SRB) cytotoxic assay was performed in MDA-MB-231 cell line.

In a 6-well plate,  $5 \times 10^5$  cells per well were plated. When cells were attached, 250 nM of aptamer were incubated with the cells for 24 h. On the day of the experiment, the medium was removed and the cells were washed with 1 mL of pre-warmed PBS 1X. To fix the cells, 1 mL of 1% (v/v) acetic acid (VWR) in methanol (Valente e Ribeiro) was added to each well and the cells were incubated for 90 min at  $-20\text{ }^\circ\text{C}$ . After cells were fixed, the 1% (v/v) acetic acid in methanol solution was removed and the plate was allowed to dry at  $37\text{ }^\circ\text{C}$  for 15 min. Then, 1 mL of 0.5 % (w/v) SRB (Sigma) in 1 % (v/v) acetic acid was added and the cells were incubated for 90 min at  $37\text{ }^\circ\text{C}$ . The SRB solution was removed and the plate was allowed to dry at  $37\text{ }^\circ\text{C}$ . To dissolve the SRB attached to the cells' proteins, 1 mL of Tris 10 mM (Fisher) was added to each well and the plate was incubated with agitation. A volume of 200  $\mu\text{L}$  of the resulting solution was transferred into a 96 well plate and the absorbance was measured at 540 nm.

### 2.2.3 Morphology Assay

In order to verify if aptamer #1 and aptamer #2 had any effect on MDA-MB-231 cell line, a morphology assay was performed. In this assay,  $1 \times 10^5$  cells per well were plated, in a 6 well plate, and were incubated overnight. In the next day, 250 nM of aptamer were incubated with the cells. During 24h, there were five check points – 0 h, 3 h, 6 h, 8 h and 24 h- in which pictures of the cells were taken by Leica D-LUX 3 camera.

## 2.3 Biotin and Amine labeled Aptamer

### 2.3.1 Polymerase Chain Reaction (PCR)

PCR is a technique used in molecular biology to amplify the number of copies of a DNA sequence, providing millions of sequences. In this case, PCR was used to amplify and add desired Biotin or Amine groups to the sequence of aptamer #1 and aptamer #2.

In order to choose the best initial quantity of aptamer template to use in the PCR (Table 2.1), an optimization using 10 ng, 20 ng and 40 ng of aptamer was performed. In this optimization step, we also optimized the temperature of annealing, as we tested 8 temperatures, ranging from

48°C to 70°C – (48°C, 49.6°C, 52.3°C, 56.2°C, 61.5°C, 65.6°C, 68.3°C and 70°C). Through gel electrophoresis, we attested which conditions were the best suited for the PCR.

Table 2.1 PCR Master Mix for 1 PCR reaction tube for both aptamer #1 and aptamer #2.

PCR Master Mix (1 reaction)	
Template	10 ng
Primer Foward	0,5 µM
Primer Reverse	0,5 µM
MgCl <sub>2</sub>	0,8 mM
Mix	1 X
H <sub>2</sub> O	Up to 20 µL

### Gel Electrophoresis

In order to verify the resulting PCR product and assure that no unwanted products were obtained, and to choose the best conditions to execute the PCR, as well as to verify if the conjugation was successful, gel electrophoresis was performed. A 3% (w/v) agarose gel was prepared. The agarose (Fisher BioReagents) was dissolved in Tris-acetate EDTA (TAE) 1X, diluted from the TAE 50X (prepared using 2 M of tris base, 5.71 % (v/v) of acetic acid and 10 % (v/v) of 0.5 M EDTA (VWR)) by heating until no powder was detectable. Afterwards, 0.0005 % (v/v) thiazole orange (Enzymatic) was added to the mixture. After the gel was polymerized, DNA ladder VI (Nzytech) was loaded as well as the samples. The run was performed at 90 V for 45 min and the gel was revealed using ChemiDoc XRS+ (BioRad).

### 2.3.2 Lambda Exonuclease

In a centrifuge microtube, 6.6 µg of DNA, 10 U of lambda exonuclease, 5 µL of 10X Exonuclease buffer (New England BioLabs) and water for molecular biology (Nzytech) to complete a volume of 50 µL were added. The mix was incubated at 37 °C for 30 min. Afterwards, the activity of the enzyme was stopped by incubating the mix for 10 min at 75°C. This procedure was followed by one of three approaches.

### 2.3.2.1 Aptamer purification

After degradation, the aptamers were purified. For this purpose, three approaches were used: Phenol/Chloroform DNA extraction, Zymoclean Gel DNA Recovery Kit and Zymoclean DNA Clean & Concentrator Kit

#### Approach 1:

##### Phenol/Chloroform DNA extraction

The same volume of phenol/chloroform (1:1) (PanReac) was added to the previous mix and the solution was centrifuged at 16830 g for 5 min. The aqueous phase was transferred into a new centrifuge microtube and 50  $\mu$ L of chloroform were added to this aqueous phase. The solution was centrifuged under the previously mentioned conditions and the aqueous phase that was obtained was transferred to a new tube. Ethanol precipitation was the chosen procedure to precipitate the desired ssDNA sequences.

Then, 0.1 volume of sodium acetate 3M pH 5.2 and 2.5 volume of ice-cold absolute ethanol (Fisher Chemical) were added to the previously obtained aqueous phase and the solution was incubated at - 80°C for 30 min. Next, it was centrifuged for 8 min at 16830 g and the supernatant was discarded. A volume of 1 mL of ethanol 70% (v/v) was added and the solution was centrifuged at 16830 g for 2 min. The resulting supernatant was discarded and the remaining ethanol was allowed to dry for several minutes at 37 °C. The resulting DNA was resuspended in water for molecular biology.

#### Approach 2:

##### Zymoclean Gel DNA Recovery Kit

Another approach using the Zymoclean Gel DNA Recovery Kit (Zymo Research) to purify the ssDNA resulting from the lambda exonuclease degradation was used. The protocol was followed according to the manufacturers' instructions. Briefly, after performing a gel electrophoresis, the desired DNA fragments were excised from the agarose gel using a razor blade and transferred into microcentrifuge tubes. To the fragments excised, 3 volumes of ADB buffer per g of agarose were added. The mixture was incubated at 55 °C for 10 min in order to completely dissolve the gel slice.

The melted agarose solution was then transferred to a column in a collection tube, contained in the kit, and centrifuged for 1 min at 16830 g. The flow-through was discarded and 200  $\mu$ L of the DNA wash buffer were added to the column which was centrifuged for 30 s at 16830 g. The flow-through was discarded. The wash step was repeated one more time and the column was placed into a new microcentrifuge tube. About 10  $\mu$ L of DNA elution buffer were added into column matrix and then the column was centrifuged for 1min to elute the DNA. After this procedure, the DNA was quantified using NanoDrop 1000 (Thermo Scientific).

### Approach 3:

#### Zymoclean DNA Clean & Concentrator Kit

As an alternative to the previous approaches, a third approach resorting to Zymoclean DNA & Concentrator - 5 Kit (Zymo Research) was chosen.

Following the exonuclease lambda inactivation by heat, 7 volumes of Binding Buffer were added to the ssDNA suspension. The solution was vortexed and then transferred into a Zymospin Column and centrifuged for 30 s at 16830 g. The flow-through was discarded. Afterwards, 200  $\mu$ L of DNA Wash buffer were added into the column and it was centrifuged in the same conditions. The flow-through was discarded and the wash step was repeated. Finally, 10  $\mu$ L of DNA Elution Buffer were added to the matrix and allowed to rest for about 1 min and then the column was transferred into a new microcentrifuge tube and centrifuged for 30 s at 16830 g. The DNA was next quantified using NanoDrop 1000.

### 2.3.3 Bioconjugation

In this step, 500 mg mL<sup>-1</sup> of the Sicastar®-greenF COOH fluorescent silica nanoparticles (Micromod) were functionalized with 1 mg mL<sup>-1</sup> of amine-terminated aptamers. In order to functionalize the silica nanoparticles, about 0.4 mg of 1-(3-Dimethylaminopropyl)-3-ethylcarbodiimide hydrochloride (EDC) (AcrosOrganics) were added to 1 mL to the nanoparticles' suspension. Then 1.1 mg of N-Hydroxysulfosuccinimide sodium salt (Sulfo-NHS) (AcrosOrganics)

were added to the previous suspension. The mixture was allowed to react for 30 min at room temperature. To stop this reaction, remove excessive salts and exchange buffer, the activated silica nanoparticles were passed through a desalting column (GE Healthcare) equilibrated in PBS 1X.

The solution containing the desired aptamers was added to the desalted nanoparticles' suspension. The resulting mixture was allowed to react for 2 h at room temperature. Then, the mixture was stored at 4 °C until it was used.

### 2.3.3.1 Characterization of the conjugated aptamer-nanoparticles

#### Flow Cytometry

The cell lines were cultured as previously described.

On the day of the experiment, the culture medium was removed and the cells were washed two times with 500 µL of pre warmed PBS 1X. After this step, 200 µL of a suspension with the nanoparticle-aptamer conjugates in PBS 1X supplemented with  $\text{Ca}^{2+}$  and  $\text{Mg}^{2+}$  was incubated in each well for 30 min at 37 °C or at 4 °C, instead. The suspension was removed and the cells were washed two times with 400 µL of pre warmed PBS 1X. With the help of cell scraper, the cells were detached and transferred into centrifuge microtubes.

#### Dynamic Light Scattering

The aptamer-nanoparticle conjugates resulting from the amine reaction were diluted in 1 mL of PBS 1X. Through Dynamic Light Scattering (DLS) it was evaluated the particle size distribution. The intensity-weighted mean value was recorded as the average of three independent measurements. The size of the aptamer silica nanoprobe in PBS 1X were measured at 25°C.

#### Microvolume Spectrophotometry and Fluorometry

To evaluate the bioconjugation of the aptamer with the silica nanoparticles, the suspension, as well as a suspension containing only the nanoparticles were measured using Nanodrop 1000 at 260 nm. First, the nanoparticles suspension was loaded, using them as blank. Then, the aptamer #1 and aptamer #2 conjugated were measured. The variation of concentration allows to determine if the aptamers were conjugated.

### 2.3.4 Aptamer -mediated pull-down assay

The protocol for identification of the target protein that is being recognized by the aptamers was performed using MDA-MB-231 cell line and the biotinylated - aptamers.

#### 2.3.4.1 Subcellular fractioning

In order to identify the possible membrane targets of the aptamers, subcellular fractioning was performed resorting to the FOCUS™ SubCell Kit (GBiosciences) according to manufacturer's instructions.

Briefly, cells were cultured in a T175 flask until they reached about 90% confluence. On the day of the experiment, the cells were detached with a cell scraper and counted using a Neubauer chamber to ascertain the number of cells.  $20 \times 10^6$  cells were used to perform this protocol. In a second phase, two days prior to the fractioning, the cells were cultured in a serum free medium to attest if any effect occurred.

Afterwards, the cells were transferred to a 15 mL centrifuge tube and centrifuged at 800 g for 1 min. The supernatant was discarded and the cells were washed with ice-cold PBS 1X. The centrifugation step was repeated with the same conditions. The supernatant was discarded and 500  $\mu$ L of ice cold SubCell Buffer I with 1% (v/v) of protease inhibitors (VWR) was added to resuspend the cells. The cell suspension was incubated on ice for 10 min. Then, using a narrow open syringe needle, the cell suspension was pulled up and down a few times to lyse the cells.

#### Membrane and Cytosolic fractions isolation

About 200  $\mu$ L of 3X SubCell Buffer II were added and the tube was inverted several times to mix. Afterwards, the suspension was centrifuged at 700 g for 10 min and the supernatant was transferred into a new centrifuge tube. The obtained supernatant was centrifuged at 12 000 g for 15 min. The supernatant from this centrifugation was transferred into an ultracentrifuge tube and was centrifuged at 100 000 g for 1 hour at 4 °C. The supernatant was transferred into a new tube, as it contained cytosolic proteins. The pellet, containing the membrane fraction, was resuspended



in 200  $\mu\text{L}$  of Dulbecco's Phosphate-Buffered Saline (955 mg of D-PBS powder were weighted and deionized water was added to make up 100 mL).

#### Nuclear fraction isolation

A volume of 300  $\mu\text{L}$  of SubCell Buffer-III was added to the first pellet obtained. Then, the suspension was centrifuged at 700 g for 5 min and the supernatant was discarded. The pellet was resuspended in 700  $\mu\text{L}$  of D-PBS.

#### Protein Quantification through Bradford Protein Assay

The Bradford protein assay was used to quantify the total protein.

A calibration curve was calculated using six bovine serum albumin (BSA) concentrations (0 mg mL<sup>-1</sup>, 0.125 mg mL<sup>-1</sup>, 0.250 mg mL<sup>-1</sup>, 0.500 mg mL<sup>-1</sup>, 1 mg mL<sup>-1</sup> and 2 mg mL<sup>-1</sup>) from a solution with an initial concentration of 2 mg mL<sup>-1</sup> (GRiSP). To 100  $\mu\text{L}$  of each concentration, 1 mL of Bradford reagent (Sigma) was added. The resulting solution was vortexed and 200  $\mu\text{L}$  were transferred into a 96-well plate. The absorbance was read at 595 nm and the calibration curve built using the software Microsoft Excel 2016.

To determine the concentration of membrane protein resulting from subcellular fraction, the same procedure was used.

#### 2.3.4.2 Aptamer-target binding assay

The membrane protein fraction was blocked with binding buffer supplemented with 20 % (v/v) of FBS (21.5 mM of MgCl<sub>2</sub>·6H<sub>2</sub>O (VWR), 24 mM of D-Glucose (Fisher) and 15 nM of BSA. D-PBS 1X was added) and incubated for 1 h at 4 °C. Then, 150 pmol of biotin-labeled aptamer was incubated overnight with the membrane protein fraction at 4 °C. The obtained protein-aptamer complexes were incubated with 20  $\mu\text{L}$  streptavidin-coated beads for 1 h at 4 °C. After the incubation time, the beads were washed with D-PBS 1X and the target bound proteins were eluted by heating at 95°C for 5 min in sodium dodecyl sulfate polyacrylamide gel electrophoresis (SDS-PAGE) sample buffer. Afterwards, the proteins were loaded into an 8% (v/v) acrylamide SDS-PAGE and then stained with Coomassie Blue (AppliChem).

In order to verify if FBS or BSA present in the Binding Buffer had any effect in the binding of the aptamers to the target, the buffer was prepared without adding either FBS or BSA. Also, two days prior to the fractioning, the cells were cultured in a serum free medium to attest if any effect occurred.

# CHAPTER 3

## RESULTS AND DISCUSSION



In previous projects, Cell-SELEX was used to select aptamers able to specifically recognize MDA-MB-231 as positive TNBC cell line using MCF-10-2A as a negative cell line for counter-selection. From that process, the aptamers with the highest number of copies ( $\geq 49$  copies) were listed (Table 3.1) and the two most frequent were chosen for the following studies herein reported and for the development of a diagnostic nanoparticle.

**Table 3.1-** List of the aptamers selected against MDA-MB-231 cell line that display  $\geq 49$  copies after the last round of Cell-SELEX. Only the random region is presented.

Aptamer ID	Random Region Sequence	No. of copies
#1	GCATCCACCGTGAATATTGTAACGCTATATGTGAGTGGCTAAGTGCACC	89
#2	ATGTTGTTGCCGGGACGCCTCCTTACCAAAGTTGGTGTCCCCACCTAC	86
#3	TCGGGTGATGGGTGGACAAAAGTTAGTAGCCGCGAGCCACTGGCCCAGT	79
#4	AATGAGTGTCCGACTAAGATCTATTTTAAGCTCGACTCGTTTGGCA	64
#5	ATGCAAGTGTGCCGCGCAAACAATGCCTCCTGCTTATTTGTGCCACCA	59
#6	CGCGGTGTTATGAGGGGACAAGTACAAATCAATGTCGCCGCGTAGCCGC	59
#7	AGGGAGGTAGCGTGCCACCAGGAGTTTTGCGCTATACGATGTTGCTGG	58
#8	GACGATGTGGTCCGCTGGAATTTTGCAGCCCGCTATATGAAATCGCCA	56
#9	GATGACTGGTCATACGCGGATAAGTATATGCTGCCACCGGAGTTGCCG	56
#10	ATGCCATACGAAGTTGCCGCGTATTCTTTGCTAACGCCACCGGAGTATG	49

### 3.1 Secondary structure

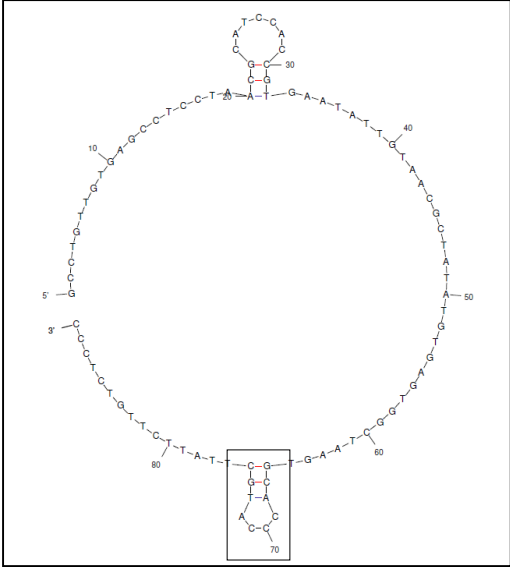
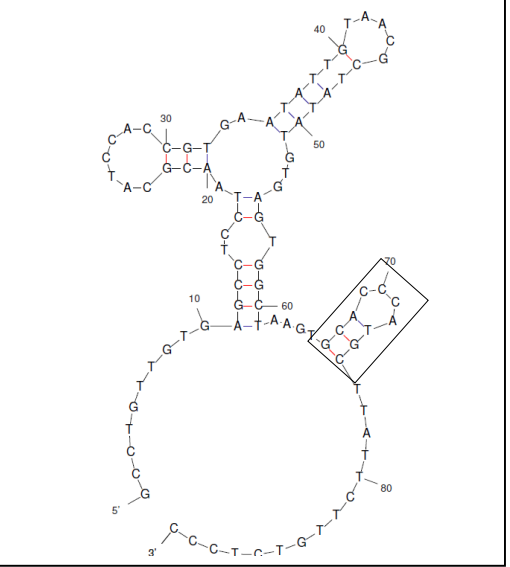
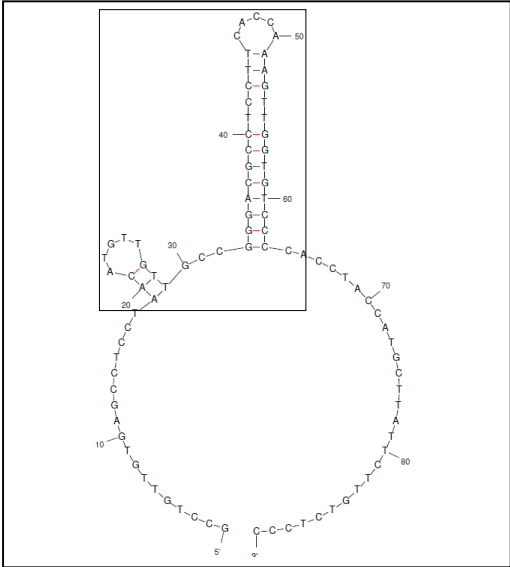
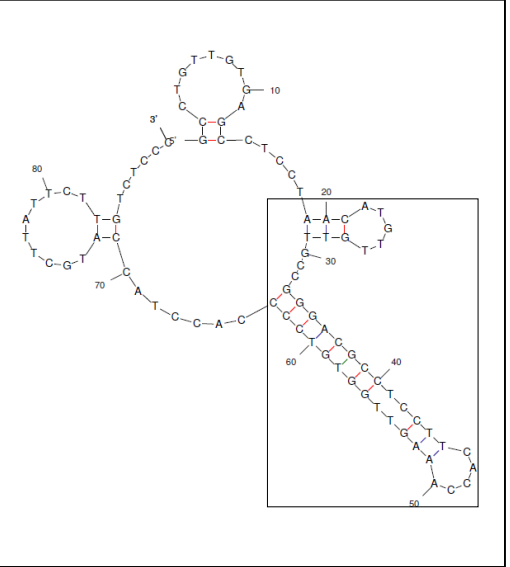
The aptamers were selected at 37 °C although they can be selected at 4 °C to target cell surface molecules, similarly to DML-7 (Duan et al., 2016). However, higher temperatures can cause aptamers to internalize, which might be desirable for different aptamer applications (Sefah et al., 2010). Aptamers selected at 37 °C can also show binding ability at 4 °C. Hence, it is important and interesting to predict its folding at both temperatures. Using the free online application DNA fold form from Mfold (The Mfold Web Server), available at <http://unafold.rna.albany.edu/?q=mfold>, we predicted the folding structure of aptamer #1 and aptamer #2 (Table 3.2).

## CHAPTER 3

### RESULTS AND DISCUSSION

According to the prediction, both aptamers have more than one possible secondary structure at 4 °C and 37 °C. Aptamer #1 has 3 possible structures at 4 °C and 37 °C and a hairpin that remains in the structure in both temperatures. As for aptamer #2, it exhibits 2 possible secondary structures at 4 °C and 37 °C and there are two hairpins preserved at each temperature.

**Table 3.2.** Prediction of the folding of aptamer #1 and aptamer #2 at 37 °C and 4 °C. Only the structure(s) with the lowest free energy (dG) are presented. The loops are marked in the black rectangles.

37 °C	4 °C
<p data-bbox="336 555 687 584">Aptamer #1 (3 potential structures)</p>  <p data-bbox="456 1200 568 1229">dG= - 1.19</p>	<p data-bbox="906 555 1257 584">Aptamer #1 (3 potential structures)</p>  <p data-bbox="1023 1200 1134 1229">dG= - 11.27</p>
<p data-bbox="336 1299 687 1328">Aptamer #2 (2 potential structures)</p>  <p data-bbox="456 1944 568 1973">dG= - 4.96</p>	<p data-bbox="906 1299 1257 1328">Aptamer #2 (2 potential structures)</p>  <p data-bbox="1023 1944 1134 1973">dG= - 16.68</p>

The secondary structures of aptamers is determined by the interactions between the nucleic acids. Complementary bases anneal due to hydrogen bonds formed between hydrogen of one base and oxygen or nitrogen in the other base, stabilizing the structure of the aptamer's sequence (Brown, 2002; Nelson & Cox, 2005).

### 3.2 *In vitro* studies

To evaluate whether aptamer #1 and aptamer #2 are able to bind to MDA-MB-231 and MCF-10-2A, flow cytometry and fluorescence microscopy were used. The results show that both aptamers are able to bind the target cell line MDA-MB-231 and that no binding occurs when the counter-selection cell line MCF-10-2A is used.

The results from flow cytometry suggest that aptamer #1 (Figure 3.1 A) binds to MDA-MB-231 cells whether incubated at 37 °C or 4 °C, with no significant difference shown. This result is also depicted for aptamer #2 (Figure 3.1 B), when incubation occurs under the same conditions. Using Mfold, it was proven that there are structures in both aptamers that do not become altered when the temperature is either 37 °C or 4 °C.



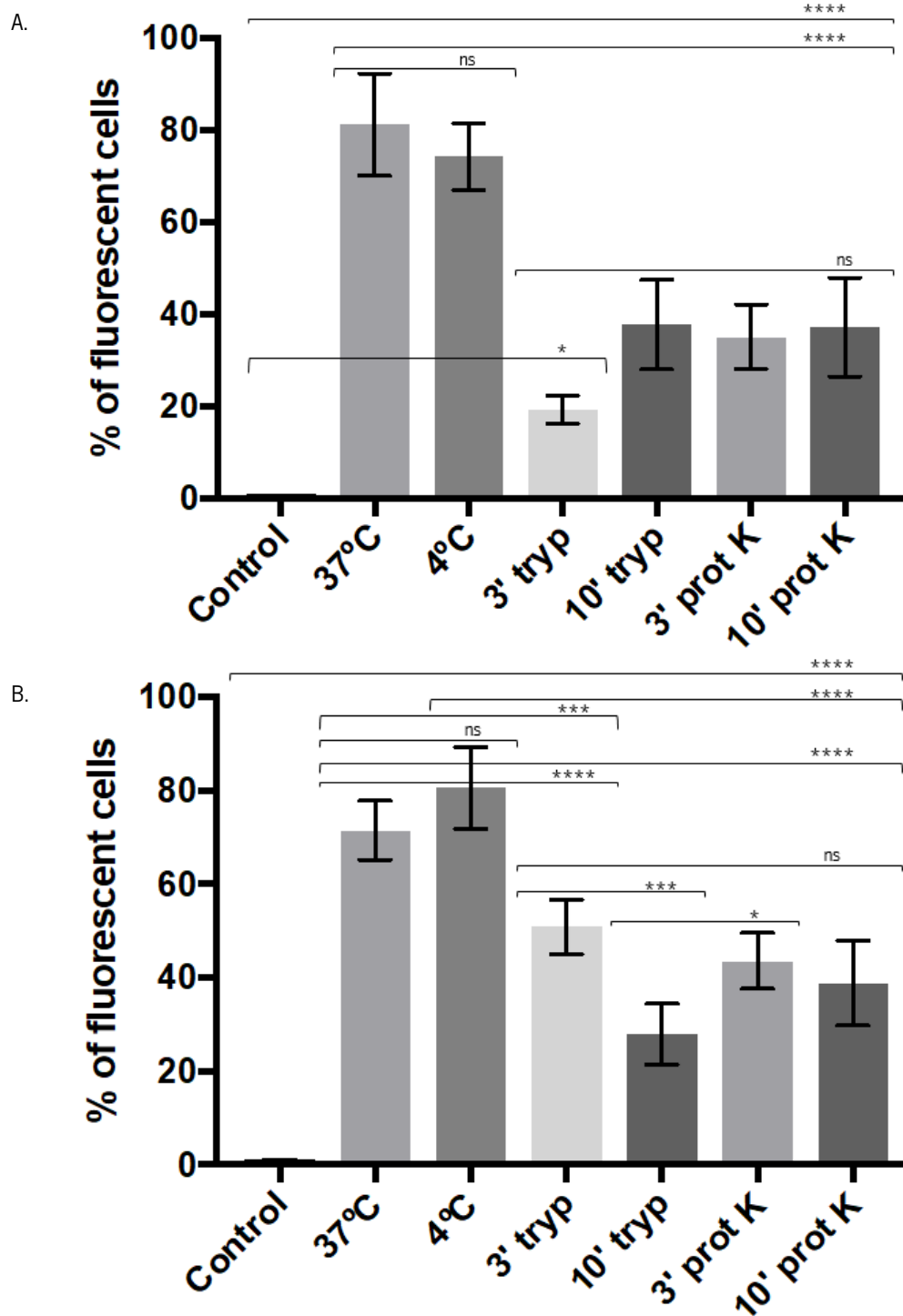


Figure 3.1. Flow cytometry binding assay using MDA-MB-231 cells for (A) aptamer #1 and (B) aptamer #2.

Comparison between control, incubation at 37 °C, 4 °C and pre-treatment with trypsin and proteinase K. ns  $P > 0.05$ ; \*  $P \leq 0.05$ ; \*\*  $P \leq 0.01$ ; \*\*\*  $P \leq 0.001$ ; \*\*\*\*  $P \leq 0.0001$ . The results are the average of % fluorescent cells for each treatment  $\pm$  standard deviation.

For cells that were first treated with trypsin or protease K and then incubated with either aptamer #1 or aptamer #2, the percentage of fluorescent cells decreases, when compared to the incubation at 37 °C. It was noticed that there was a significant decrease when comparing the results from treatment with trypsin for 3 min and 10 min before incubating with aptamer #2. Once Cell-SELEX was performed at 37 °C, it was possible for the selected aptamers to internalize (W. Li et al., 2014). Hence, herein cells were treated with either trypsin or proteinase K. After evaluating the results from pre-treated cells with no treated cells, it was found that both aptamers could be internalized by MDA-MB-231. Probably the aptamers bind to an intracellular receptor that is also present in the cellular membrane. However, it is important to note that aptamers may preferably bind the cell membrane target, given that the untreated cells showed higher fluorescence. Additionally, comparing the results for cells treated for 10 min with trypsin and cells treated for 3 min with trypsin, a significant decrease in fluorescence was found for the cells incubated for the longer period with the treatment agent. These results may be due to several factor including for instance differences in the isolation of the cells, comparing to other wells from different treatments, loss of cells as trypsin is used to detach cells and perform subculturing, and damage of the cells because of trypsin.

Incubation of MDA-MB-231 cells with the library was also performed under the selection conditions. The results obtained were compared to the ones from incubation with aptamer #1 and aptamer #2, as well as with untreated cells (Figure 3.2). According to the results, there is significant difference of the % of fluorescent cells between the control and cells incubated with library. There is a very significant difference between cells incubated with aptamers and with library. Such result indicates that there are sequences present in the library that show affinity for MDA-MB-231 cells, although their ratio can be low.

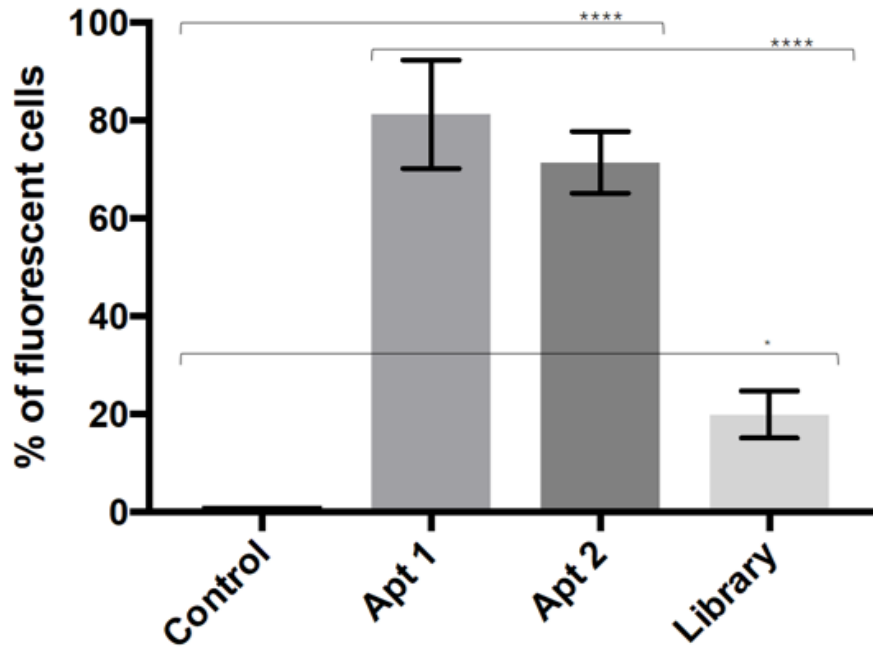


Figure 3.2. Flow cytometry binding assay with MDA-MB-231 for library. Comparison between control, aptamer #1, aptamer #2 and library. ns  $P > 0.05$ ; \*  $P \leq 0.05$ ; \*\*  $P \leq 0.01$ ; \*\*\*  $P \leq 0.001$ ; \*\*\*\*  $P \leq 0.0001$ . The results are the average of % fluorescent cells for each treatment  $\pm$  standard deviation.

In what concerns the flow cytometry using MCF-10-2A, results confirmed that no significant fluorescence was observed when incubated with aptamer #1, aptamer #2 or library (Figure 3.3), as expected.

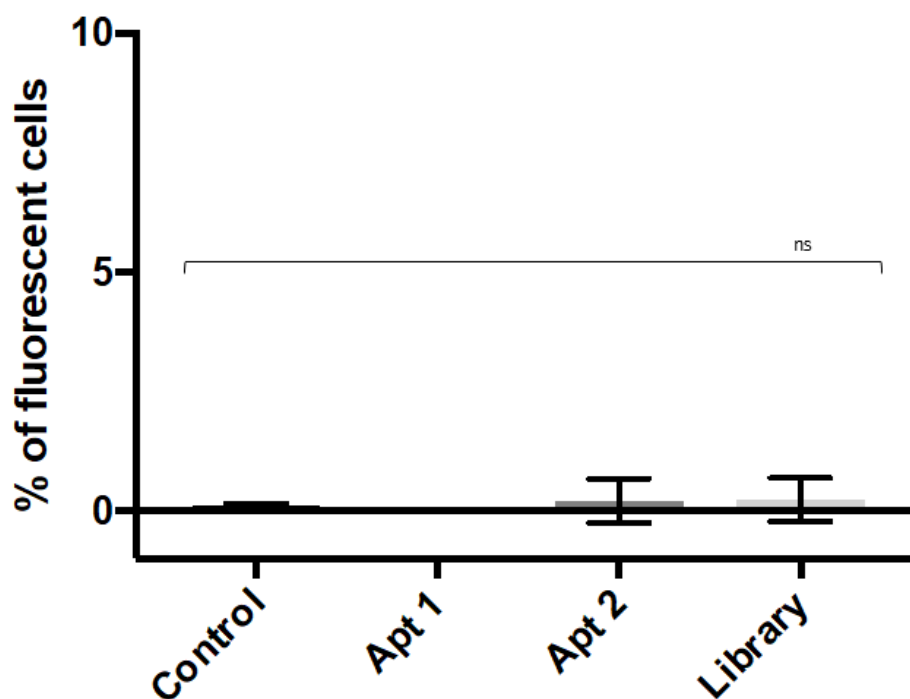


Figure 3.3. Flow cytometry binding assay for MCF-10-2A. The cells were incubated with aptamer #1, aptamer #2 and library. ns  $P > 0.05$ ; \*  $P \leq 0.05$ ; \*\*  $P \leq 0.01$ ; \*\*\*  $P \leq 0.001$ ; \*\*\*\*  $P \leq 0.0001$ . The results are the average of % fluorescent cells for each treatment  $\pm$  standard deviation.

MDA-MB-231 cells were incubated with aptamer #1 and aptamer #2 and then observed through fluorescence microscopy (Figure 3.4). The fluorescence microscopy images confirmed the results attained in the flow cytometry experiments; i.e. MDA-MB-231 cells exhibited fluorescence when incubated with both aptamer #1 or aptamer #2. Incubation of MDA-MB-231 cells with library did not reveal fluorescence.

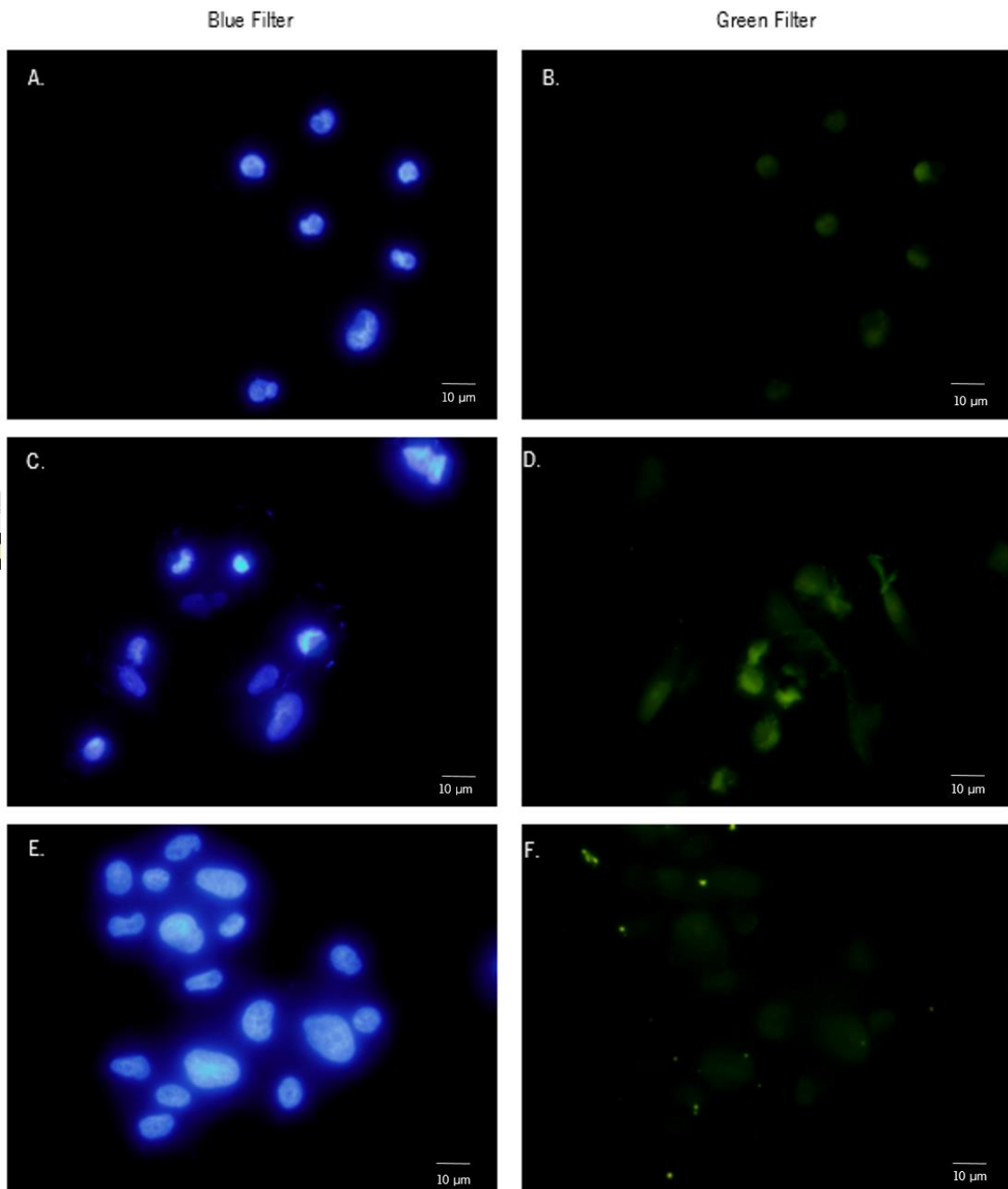


Figure 3.4. Fluorescence microscopy images of MDA-MB-231 cells incubated with aptamer #1 (A and B), aptamer #2 (C and D) and library (E and F). (A, C, E) Blue: nuclei stained with DAPI; (B, D, F) Green: represent cells stained with fluorescent aptamer.

As expected, these results are in accordance with the results of flow cytometry since the selection was performed using MDA-MB-231 cells and counter-selection was performed using MCF-

10-2A cells. Hence, it can be concluded that both aptamer #1 and aptamer #2 recognize and specifically bind to a TNBC cell line and the library does not seem to display the same ability to bind the target cell line.

### 3.2.1 $K_D$ determination using flow cytometry

In order to determine the  $K_D$ , MDA-MB-231 cells were incubated with several concentrations of aptamer #1 and aptamer #2. Then, using GraphPad Prism 7, the  $K_D$  of each aptamer was determined. Both aptamers presented a  $K_D$  in the nM range (Figure 3.5); aptamer #1  $K_D$  was  $82.29 \pm 13.64$  nM and aptamer #2  $K_D$  was  $54.63 \pm 18.87$  nM. Both aptamers revealed high affinity to the target MDA-MB-231 cells, as their  $K_D$  is close to 50 nM, i.e, the mid nM range (Gold et al., 2010; Sefah et al., 2010). The results show that the Cell-SELEX initially performed was successful and the selected aptamers bind to the target TNBC cell line and do not recognize the control cell line.

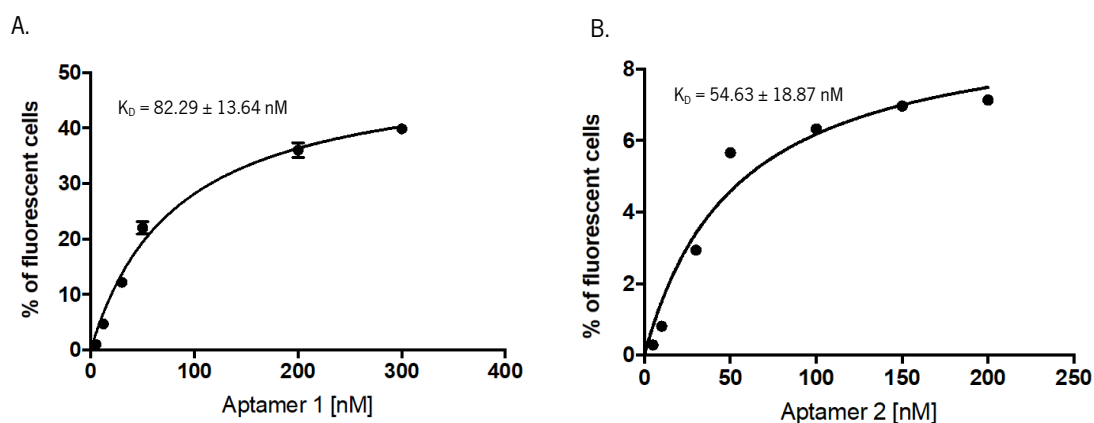


Figure 3.5. Kinetics curve of (A) aptamer #1 and (B) aptamer #2 and their respective  $K_D$ . Flow cytometry was used to determine the binding affinities of the aptamers selected against MDA-MB-231 cells.

Li and team (2014) selected a set of aptamers against MDA-MB-231 cells. The  $K_D$  of their aptamers was determined through flow cytometry. It is interesting that of the aptamers characterized, two have similar  $K_D$  to our aptamer #1 and aptamer #2. Aptamer LXL-1 possessed

a  $K_D$  of  $44 \pm 8$  nM and aptamer LXL-7 a  $K_D$  of  $108 \pm 32$  nM, values that are in the same range of the ones herein calculated for aptamer #2 and aptamer #1, respectively.

### 3.3 Biotin and amine labeled aptamers

In order to recognize the putative target of the aptamers and to functionalize the fluorescent silica nanoparticles, PCR using biotin and amine labeled forward primers was performed at 52.3 °C. Then, it was degraded by lambda exonuclease.

In the first approach for purification, the DNA resulting from the degradation was extracted through phenol/chloroform and then ethanol precipitated. Through gel electrophoresis (Figure 3.6), it was verified that the extraction method did not lead to the desired ssDNA, and no DNA bands could be identified. It is possible that the DNA remained in the organic phase, lowering the amount of DNA recovered. Moreover, this is a time consuming method, which can increase the risk of DNA loss, although it is the most appropriated method to clean-up the samples after a digestion (Smolke Lab). Therefore, DNA extraction kits were used to purify the ssDNA aptamers.

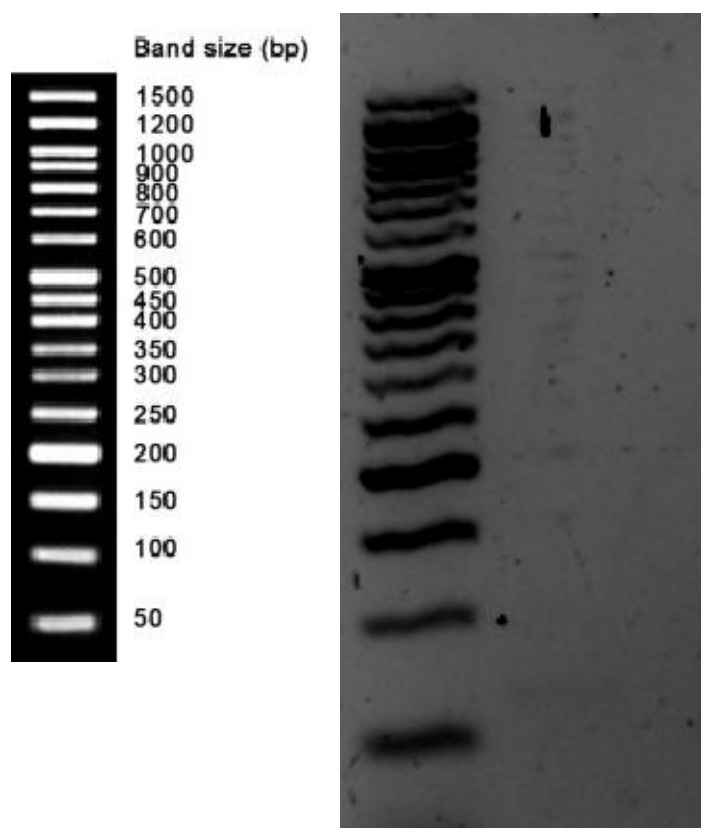


Figure 3.6. Gel agarose from digestion of ds aptamer #1 to ss aptamer #1 and subsequent extraction through phenol/chloroform and purification with ethanol.

Although the kits are designed for samples containing between 50 bps and 23 thousand bps, a low amount of DNA was obtained. Moreover, eventually the aptamers are small enough to pass through the column or even the elution buffer was not incubated for enough time before the final elution.

### 3.3.1 Aptamer-based pull-down

After confirming that both aptamers were able to bind to MDA-MB-231 cells and that the target of each aptamer was present in the cell membrane, as well as inside the cell, fractioning of the cell was attempted using a kit. The membrane, cytosol and nuclear fractions of MDA-MB-231 cells were obtained and incubated with the aptamers as suggested by Wang and co-workers (



2017). In a first approach, binding buffer containing BSA and FBS was used. However, its composition was changed due to the fact that these affected the results (see Appendix, Figures A.2 and A.3). Very strong bands were observed. This indicated a possible contamination with, probably and most likely BSA, as this protein's molecular weight is 66 kDa. In another repetition of the assay using the binding buffer without FBS and BSA, it was observed that the beads did not have any effect in the cellular fractions, and were removed.

After SDS-PAGE electrophoresis (Figure 3.7), no bands were observed on incubation with the nuclear fraction. As for cytosol and membrane fractions (Figure 3.8 A and B, respectively), a thin band between 63 and 75 kDa was observed in both aptamers. Moreover, it was noted that the bands observed were the same for both aptamers and for both cytosolic and membrane fractions. This result can indicate that the target of both aptamer #1 and aptamer #2 is the same. With the introduction of the new buffer, no detectable contaminants were found.

Strande and co-workers (2009) explored the proteome of MDA-MB-231 cells. Using their results, 4 possible targets were found for aptamer #1 and aptamer #2 (Table 3.3).

The possible targets' role is important for the cell to function and maintain itself alive, once tasks as crucial as response to insulin or motility and mitosis. According to the literature, none of these proteins are expressed exclusively in breast cells, except for radixin, whose expression is not described yet.

To ensure which is the target for the aptamer, another method such as sequencing or molecular docking could be employed.

## CHAPTER 3

### RESULTS AND DISCUSSION

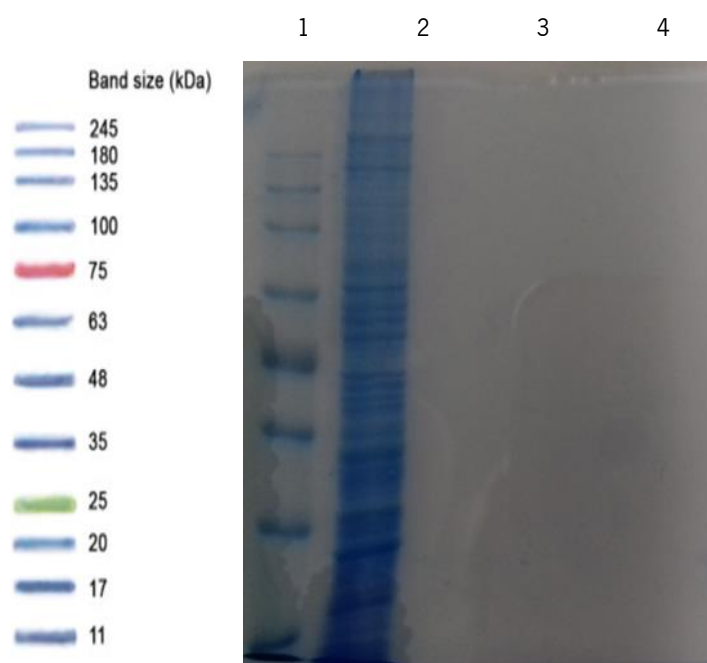
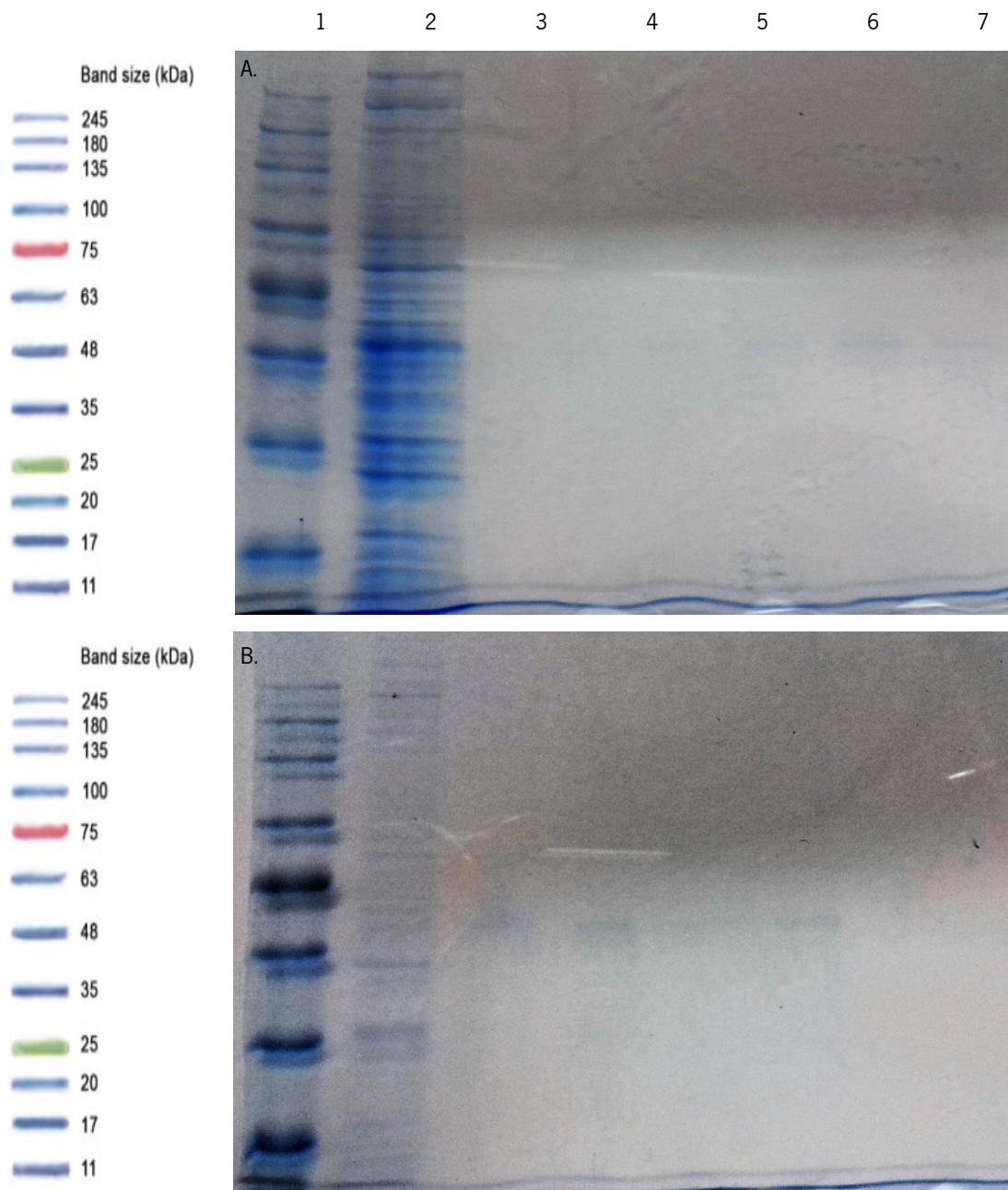


Figure 3.7. SDS-PAGE gel from pull-down assay from nuclei fraction. (1) Biomarker, (2) nuclear fraction, (3) nuclear fraction incubated with aptamer #2 at 37 °C, (4) nuclear fraction incubated with aptamer #2 at 4 °C.

Taking into account the results obtained in the *in vitro* studies, it was expected to be able to isolate a possible target from the membrane and the cytosol fraction.



**Figure 3.8.** SDS-PAGE gels from pull-down assay from (A) cytosolic fraction and (B) membrane fraction of MDA-MB-231. A: (1) Biomarker, (2) cytosol fraction, (4) cytosol fraction incubated with aptamer #1 at 37 °C, (5) cytosol fraction incubated with aptamer #1 at 4 °C, (6) cytosol fraction incubated with aptamer #2 at 37 °C, (7) cytosol fraction incubated with aptamer #2 at 4 °C. B: (1) Biomarker, (2) membrane fraction, (3) membrane fraction incubated with aptamer #1 at 37 °C, (4) membrane fraction incubated with aptamer #1 at 4 °C, (5) membrane fraction incubated with aptamer #2 at 37 °C, (6) membrane fraction incubated with aptamer #2 at 4 °C.

GR-3 aptamer was selected through Cell-SELEX and its target was isolated using aptamer-mediated pull-down. In this case, Western blotting allowed to confirm the target, which was GCGR, an already known target that is crucial in diabetes mellitus (G. Wang et al., 2017). For aptamer #1 and aptamer #2 it was not possible to follow this route, as no TNBC biomarkers are currently known. Therefore, the possible target needs to be sequenced.

Table 3.3 Possible targets of aptamer #1 and aptamer #2 on MDA-MB-231 cell line.

Protein	Molecular weight (Da)	Function
Radixin	68635.43	Probably plays a crucial role in the binding of the barbed end of actin filaments to the plasma membrane (Hoefflich & Ikura, 2004)
Syntaxin-binding protein 1	67925.01	May participate in the regulation of synaptic vesicle docking and fusion, possibly through interaction with GTP-binding proteins. Essential for neurotransmission (Helbig, 2015)
Clathrin interactor 1	68272.82	Binds to membranes enriched in phosphatidylinositol 4,5-bisphosphate (PtdIns(4,5)P <sub>2</sub> ). May have a role in transport via clathrin-coated vesicles from the trans-Golgi network to endosomes. Stimulates clathrin assembly (Koltzsch, Neumann, Kö, & Gerke, 2003; Mills et al., 2003)
Cdc42 – interacting protein 4	68538.29	Required for translocation of GLUT4 to the plasma membrane in response to insulin signalling. Required to coordinate membrane tubulation with reorganization of the actin cytoskeleton during endocytosis. Binds to lipids, promotes membrane invagination and the formation of tubules. Promotes CDC42-induced actin polymerization. Required for the formation of podosomes, actin-rich adhesion structures specific to monocyte-derived cells (Itoh et al., 2005; Linder, Hüfner, Wintergerst, & Aepfelbacher, 2000; Qian et al., 2006)

### 3.3.2 Cytotoxicity evaluation

As confirmed above, these aptamers are able to target proteins present in the membrane, as well as in the cytosol. SRB assay was performed to assess if both aptamers and also SiNPs produce any effect on the MDA-MB-231 cells. The results (Figure 3.9) suggest that both aptamer #1 and aptamer #2 affect negatively the cells, yet not highly significant.

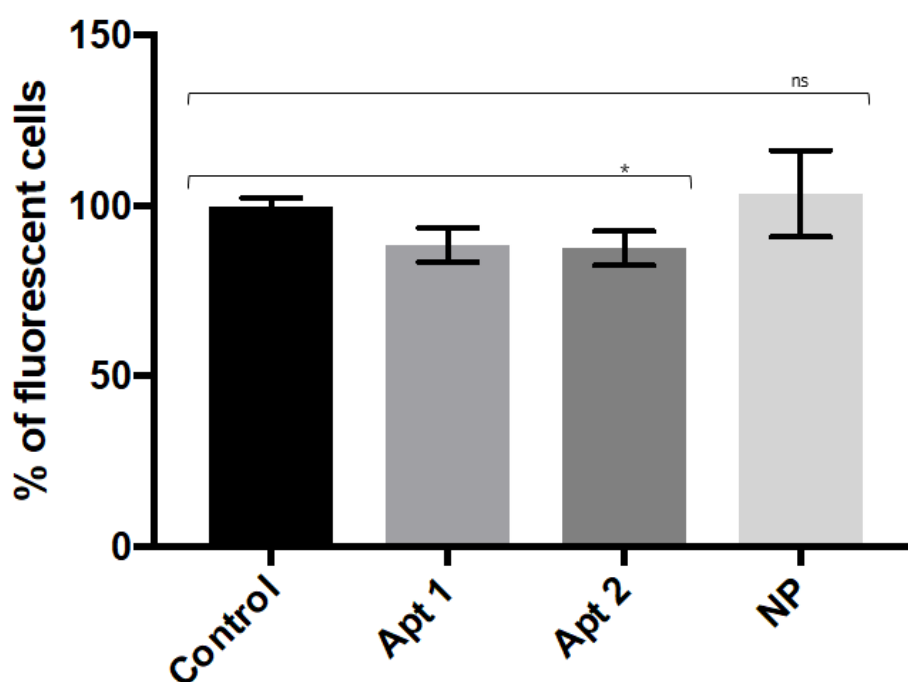


Figure 3.9. SRB assay for MDA-MB-231 cells. ns  $P > 0.05$ ; \*  $P \leq 0.05$ ; \*\*  $P \leq 0.01$ ; \*\*\*  $P \leq 0.001$ ; \*\*\*\*  $P \leq 0.0001$ .

The results are the average of % fluorescent cells for each treatment  $\pm$  standard deviation.

Although the aptamers did not show a highly significant effect on MDA-MB-231 cells, their effect was confirmed. AS1411 exhibits an antiproliferative activity (Bates et al., 1999).

To further explore the possible effects of the aptamers on MDA-MB-231 cells, a morphology assay was performed.

### 3.3.3 Morphology assay

The SRB assay indicated a possible negative effect from aptamer #1 and aptamer #2 on MDA-MB-231 cells, therefore a morphology assay was performed. For that purpose, 250 nM of

## CHAPTER 3

### RESULTS AND DISCUSSION

each aptamer was incubated with the cells, whose morphology was supervised regularly. When comparing the images (Figure 3.10), it looks like the aptamers did not affect the morphology of the cells, although the SRB indicated that the aptamers do affect their viability. Therefore, it would be interesting to repeat both assays. For the morphology assay, the time of the assay should be extended to 48 h or even 72 h, as a longer period could be necessary for the aptamers to produce their effect. Regarding the SRB assay, the results are less accurate as they rely on a dye that binds to the proteins, which can vary, among other factors, with the number of cells and manipulation problems (Orellana & Kasinski, 2016).

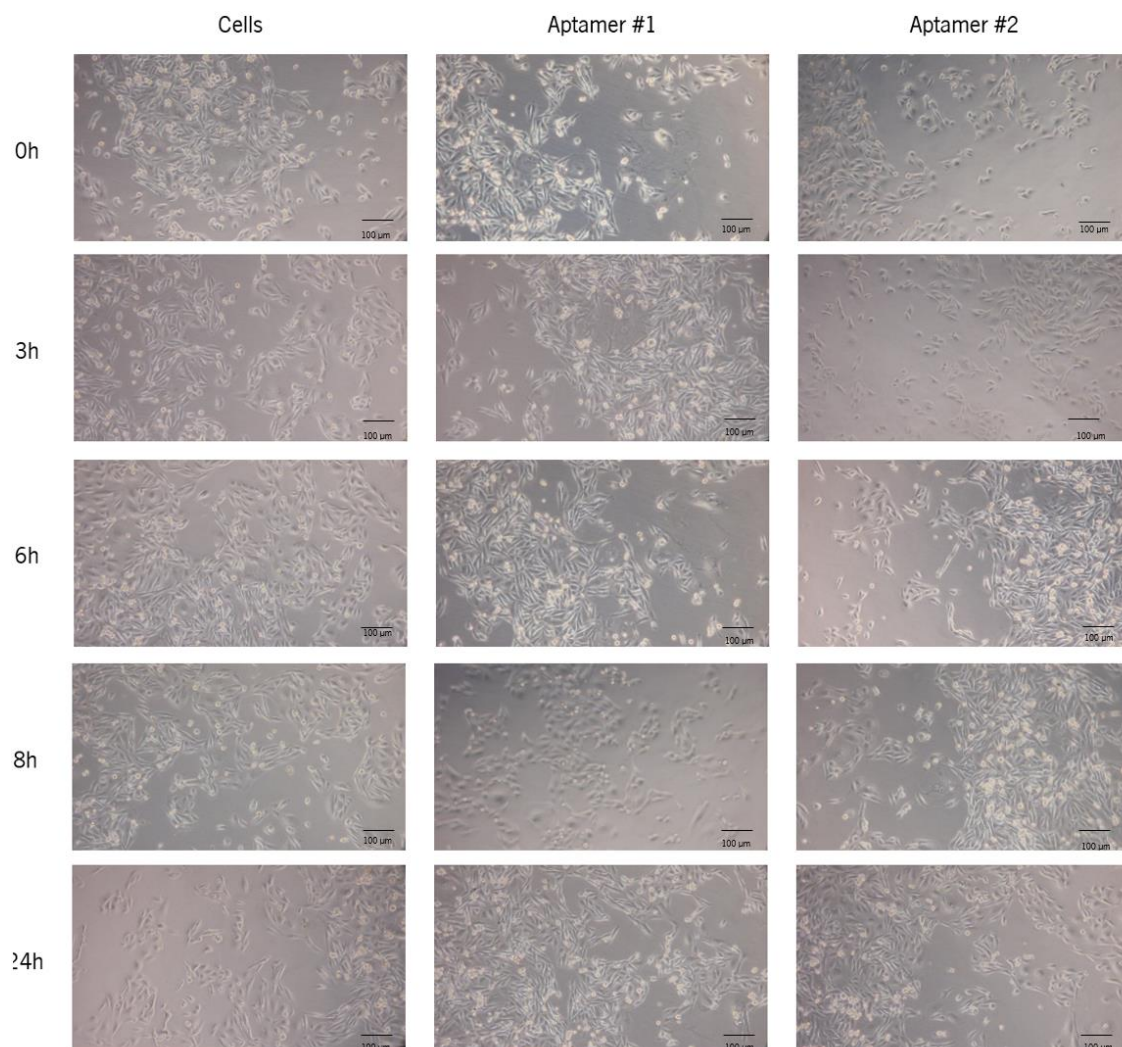


Figure 3.10. Morphology assay for MDA-MB-231 incubated with no aptamer, with aptamer #1 and aptamer #2 at 0h, 3h, 6h, 8h and 24h after incubation.

### 3.3.4 Bioconjugation

To assess the possibility of using the aptamers as diagnostic tools, the oligonucleotides were conjugated with SiNPs. The success of the conjugation procedure was confirmed through the analysis of the samples by DLS, NanoDrop 1000 and gel electrophoresis.

#### 3.3.4.1 Characterization of aptamer-nanoparticle conjugates

Through DLS, the diameter of SiNPs was determined to be  $74.51 \pm 5.12$  nm, which is around 70 nm, as stated by the manufacturer (Installation, 2017). Then, the aptamer-SiNPs samples were measured, as well as the SiNPs, however exposed to the same treatment as the conjugates. The aptamer #1 – SiNPs average diameter was found to be  $536.63 \pm 8.97$  nm; aptamer #2 – SiNPs average diameter was  $909.33 \pm 79.29$  nm. SiNPs that suffered the same treatment as the conjugates possessed a diameter of  $1117 \pm 79.93$  nm.

The results fail to meet the expected diameter. Given that even the SiNPs that suffered the bioconjugation treatment (but without aptamers bound) showed a different diameter than the one described by the manufacturer, it is possible that the protocol used promoted aggregation of the SiNPs at some point. Once the diameter estimated by DLS was greater than the one described and aggregation might have occurred, it was not possible to evaluate if the aptamers were conjugated with the nanoparticles. The samples could have been sonicated to prevent aggregation (Modrejewski et al., 2016).

Jo and collaborators (2015) described SiNPs conjugated with aptamers of similar length to the aptamer #1 and aptamer #2, which diameter was  $89.34 \pm 2.01$  nm, a value closer to the one that should have been registered. The SiNPs used for conjugation had a diameter of 70 nm (Jo et al., 2015).

Since it was not possible to confirm the success of the bioconjugation through DLS, the samples absorbance at 260 nm was measured by NanoDrop. The concentration value should increase when the conjugated samples were loaded and should be close to zero when SiNPs samples ( $0.4 \pm 0.3$  ng  $\mu\text{L}^{-1}$ ) were loaded, as the last ones were used as blank samples. For the conjugated aptamer #1 and aptamer #2, the concentration estimated was around zero. The results

attained suggest that no aptamers were conjugated. Hence, another method was used to confirm the occurrence of conjugation.

The third approach to attempt to determine if conjugation occurred was gel electrophoresis with a 3% agarose gel. After revealing the gel on ChemiDoc XRS+, no bands were visible on the aptamer #1 and aptamer #2 lanes (Figure 3.11). At the top of the gel, in the wells, there is a blur, which is caused by the nanoparticles that cannot migrate through the gel.

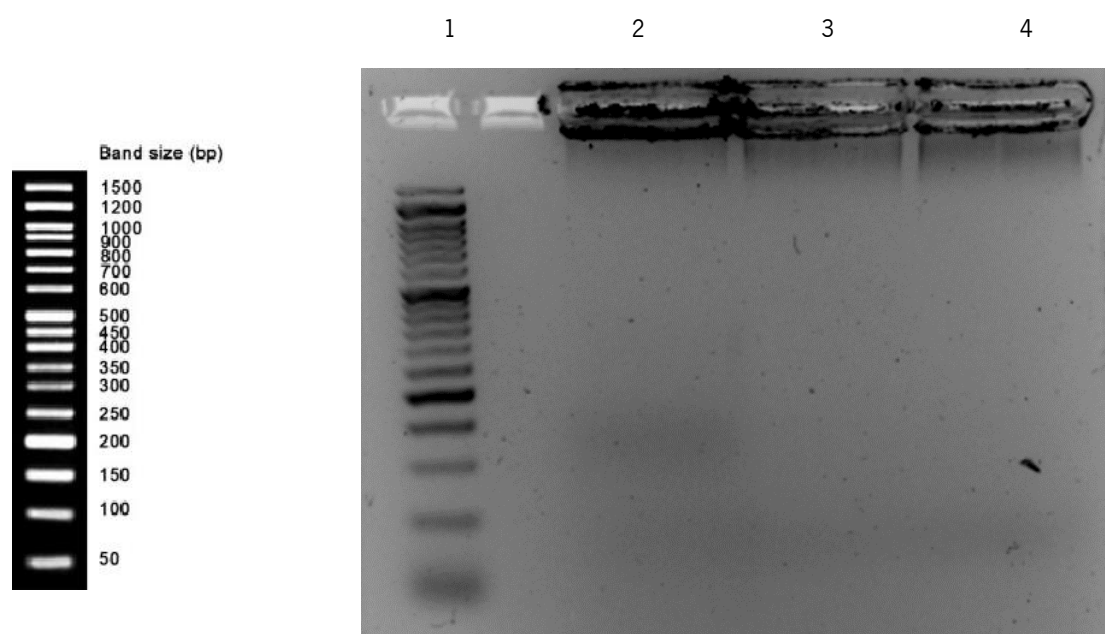


Figure 3.11. Gel electrophoresis to confirm the functionalization of aptamer displaying (1) biomarker, (2) aptamer #1 conjugated with SiNPs, (3) aptamer #2 conjugated with SiNPs and (4) SiNPs.

According to Modrejewski and co-workers (2016), this approach does allow to confirm the functionalization as a band should appear at 90 bp for both aptamers, in this case, and no band should be visible in the SiNPs lane. The fact that no bands are visible, although a sufficient amount of ssDNA was loaded, together with the presence of the nanoparticles in the wells could indicate that the DNA was not able to migrate through the gel. The aptamers could still be bound to the nanoparticles and/or the amount of aptamer that migrated was not enough and could be under the detection limit of ChemiDoc XRS+.



### 3.3.4.2 Binding

Although the functionalization was not confirmed through the proposed methods previously discussed, flow cytometry and microscopy assays were performed.

The flow cytometry results (Figure 3.12) show that aptamer #1 and aptamer #2 conjugated and free SiNPs exhibited 98.65 %, 98.88 % and 98.37 % of fluorescent cells, respectively, with no significant differences found between them.

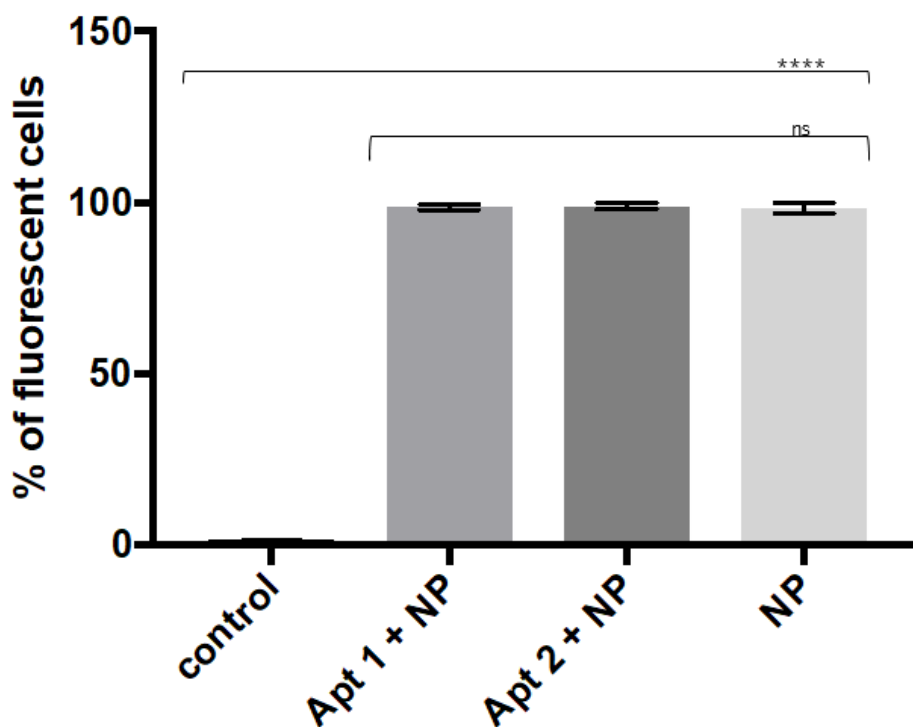


Figure 3.12. Flow cytometry for MDA-MB-231 cells incubated with aptamer #1 conjugated, aptamer #2 conjugated and free SiNPs. ns  $P > 0.05$ ; \*  $P \leq 0.05$ ; \*\*  $P \leq 0.01$ ; \*\*\*  $P \leq 0.001$ ; \*\*\*\*  $P \leq 0.0001$ . The results are the average of % fluorescent cells for each treatment  $\pm$  standard deviation.

The observation of the cells through fluorescence microscopy (Figure 3.13) confirmed the presence of fluorescence, as seen through flow cytometry.

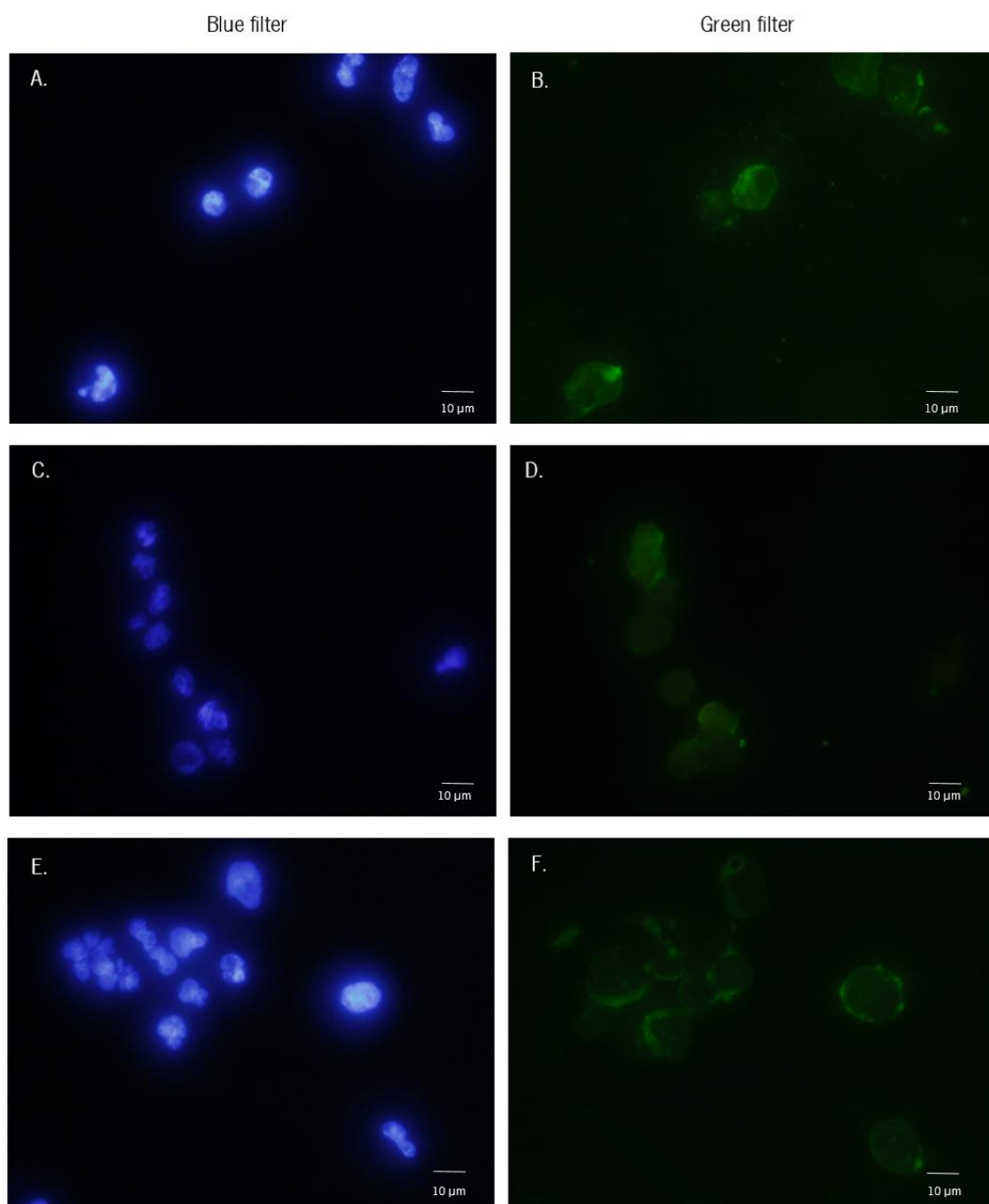


Figure 3.13. Fluorescence microscopy of MDA-MB-231 cells incubated with SiNP conjugated with aptamer #1 (A and B), SiNP conjugated with aptamer #2 (C and D) and SiNPs (E and F). (A, C, E) Blue, nuclei stained with DAPI, (B, D, F). Green, represents cells stained with SiNP.

Analyzing the flow cytometry and fluorescence microscopy results and keeping in mind that the SiNPs' diameter is 70 nm, it is possible that the SiNPs' functionalized entered the cell

through endocytosis (Oh & Park, 2014). Since we could not confirm at this stage that the aptamers were conjugated, the nanoparticles could only enter the cells through non-mediated endocytosis, which is non-specific and implies that any cell type, TNBC or not, would take up the nanoparticles and exhibit fluorescence.

Overall, results herein gathered demonstrated that aptamer #1 and aptamer #2 were able to recognize a TNBC cell line, to which they are capable of binding with high affinity, on a target that is present in the cell membrane and in the cytosol. The target of the aptamers was isolated and purified through an aptamer-pull down assay. It is possible that this is the target for both aptamers, although the aptamers are different, once the bands on SDS-PAGE gel appear in the same size. As for the conjugation, it was not possible to confirm the successful conjugation of the aptamer with a nanoparticle, as initially proposed.



## CHAPTER 4

CONCLUSIONS AND RECOMENDATIONS FOR FUTURE WORK



The goal of the experimental work was to develop an aptamer-based nanoparticle that allows to diagnose TNBC, using aptamers previously selected through Cell-SELEX. The selection was targeted against MDA-MB-231 cells and MCF-10-2A was the counter-selection cell line used.

The secondary structure of the aptamers was predicted *in silico*, and it was observed that both presented a structure that was present at 4 °C and 37 °C. This could be the structure that binds to the target in the studied cells.

Aptamers labeled with FAM were tested to assess whether they were able to bind the target and the non-target cells. Aptamer #1 and Aptamer #2 did bind to MDA-MB-231 cells and did not exhibit binding ability for MCF-10-2A. Incubation of the aptamers with MDA-MB-231 cells was conducted at 37 °C and 4 °C. The cells were also subjected to a pre-treatment with trypsin and protease K in order to attest if aptamers were able to internalize, which was confirmed. The library was also evaluated for ability to bind the target cells. It was found that the affinity shown was significant.

$K_D$  of each aptamer was determined and demonstrated high affinity towards the target MDA-MB-231 cell line. This means that both aptamer #1 and aptamer #2 are successful probes selected through Cell-SELEX and both can be further used to achieve functionalized SiNPs.

The SiNPS were functionalized using the carbodiimide chemistry. The different methods used did not confirm conjugation. Yet, the binding ability of the conjugates was evaluated and indicated that the SiNPs entered the cells, which might be due to their size.

The toxicity assay performed suggested that the aptamers did affect the cells, although the cells' morphology did not change.

The targets to which aptamers bind were isolated and, analyzing the gel, it seems to be the same; the bands on the SDS-PAGE gel showed, approximately, the same molecular weight.

A few modifications could be made to the experimental work in order to further improve the results herein generated. Regarding conjugation, it can be improved by raising the concentration of aptamer used, which was not possible because the amount of aptamer obtained from the activity of lambda exonuclease and purification was low. A greater concentration of

aptamer would increase the probability of aptamer to encounter the nanoparticle and bind to it, which could then be confirmed by the approaches above.

After obtaining the conjugates, the ligation could be characterized with respect to photostability, size, surface charge, surface functionality, optical and spectral features as well as morphology.

Further analysis of the effects in the morphology are advised, in order to confirm the potential effect and toxicity.

In conclusion, the results herein gathered demonstrated that Cell-SELEX is a useful tool to select aptamers with the ability to recognize and bind specifically to a TNBC cell line. If the improvements referred are implemented, it will be possible to develop a nanoparticle that allows the diagnosis of TNBC through imaging systems.



## REFERENCES



## Articles:

- Akbarzadeh, A., Samiei, M., & Davaran, S. (2012). Magnetic nanoparticles: preparation, physical properties, and applications in biomedicine. *Nanoscale Research Letters*, *7*(1), 144. <https://doi.org/10.1186/1556-276X-7-144>
- Alshaer, W., Hillaireau, H., Vergnaud, J., Mura, S., Deloménie, C., Sauvage, F., Ismail, S., Fattal, E. (2018). Aptamer-guided siRNA-loaded nanomedicines for systemic gene silencing in CD-44 expressing murine triple-negative breast cancer model. *Journal of Controlled Release*, *271*(October 2017), 98–106. <https://doi.org/10.1016/j.jconrel.2017.12.022>
- Arap, W., Pasqualini, R., Montalti, M., Petrizza, L., Prodi, L., Rampazzo, E., Zaccheroni, N., Marchiò, S. (2013). Luminescent silica nanoparticles for cancer diagnosis. *Current Medicinal Chemistry*, *20*(17), 2195–211. Retrieved from <http://www.ncbi.nlm.nih.gov/pubmed/23458621>
- Bagalkot, V., Zhang, L., Levy-Nissenbaum, E., Jon, S., Kantoff, P. W., Langer, R., & Farokhzad, O. C. (2007). Quantum dot - Aptamer conjugates for synchronous cancer imaging, therapy, and sensing of drug delivery based on Bi-fluorescence resonance energy transfer. *Nano Letters*, *7*, 3065–3070. <https://doi.org/10.1021/nl071546n>
- Bamrungsap, S., Chen, T., Shukoor, M. I., Chen, Z., Sefah, K., Chen, Y., & Tan, W. (2012). Pattern recognition of cancer cells using aptamer-conjugated magnetic nanoparticles. *ACS Nano*, *6*(5), 3974–3981. <https://doi.org/10.1021/nn3002328>
- Barman, J. (2015). Targeting cancer cells using aptamers: Cell-SELEX approach and recent advancements. *RSC Advances*, *5*(16), 11724–11732. <https://doi.org/10.1039/c4ra12407c>
- Bazak, R., Houry, M., Achy, S. El, Kamel, S., Officer, H., Refaat, T., ... Lurie, R. H. (2016). Cancer active targeting by nanoparticles: a comprehensive review of literature. *Journal of Cancer Research and Clinical Oncology*, *141*(5), 769–784. <https://doi.org/10.1007/s00432-014-1767-3>.Cancer
- Bozzuto, G., & Molinari, A. (2015). Liposomes as nanomedical devices. *International Journal of*

## REFERENCES

- Nanomedicine*, 10, 975–999. <https://doi.org/10.2147/IJN.S68861>
- Cailleau, R., Young, R., Olivé, M., & Reeves, W. J. J. (1974). Breast Tumor Cell Lines From Pleural Effusions. *Journal of the National Cancer Institute*, 53(3), 661–674. <https://doi.org/10.1017/CBO9781107415324.004>
- Camorani, S., Crescenzi, E., Fedele, M., & Cerchia, L. (2018). Oligonucleotide aptamers against tyrosine kinase receptors: Prospect for anticancer applications. *Biochimica et Biophysica Acta - Reviews on Cancer*, 1869(2), 263–277. <https://doi.org/10.1016/j.bbcan.2018.03.003>
- Chinen, A. B., Guan, C. M., Ferrer, J. R., Barnaby, S. N., Merkel, T. J., & Mirkin, C. A. (2015). Nanoparticle Probes for the Detection of Cancer Biomarkers, Cells, and Tissues by Fluorescence. *Chemical Reviews*, 115(19), 10530–10574. <https://doi.org/10.1021/acs.chemrev.5b00321>
- Chu, T. C., Twu, K. Y., Ellington, A. D., & Levy, M. (2006). Aptamer mediated siRNA delivery. *Nucleic Acids Research*, 34(10), 1–6. <https://doi.org/10.1093/nar/gkl388>
- Chua, C. Y. X., Jain, P., Susnjar, A., Rhudy, J., Folci, M., Ballerini, A., ... Grattoni, A. (2018). Nanofluidic drug-eluting seed for sustained intratumoral immunotherapy in triple negative breast cancer. *Journal of Controlled Release*, 285(June), 23–34. <https://doi.org/10.1016/J.JCONREL.2018.06.035>
- Crown, J., O'Shaughnessy, J., & Gullo, G. (2012). Emerging targeted therapies in triple-negative breast cancer. *Annals of Oncology*, 23(SUPPL. 6). <https://doi.org/10.1093/annonc/mds196>
- Dawood, S. (2010). Triple-Negative Breast Cancer. *Drugs*, 70(17), 2247–2258. <https://doi.org/10.2165/11538150-000000000-00000>
- Duan, M., Long, Y., Yang, C., Wu, X., Sun, Y., & Li, J. (2016). Selection and characterization of DNA aptamer for metastatic prostate cancer recognition and tissue imaging. *Oncotarget*, 7(24).

- Dunne, M., Dou, Y. N., Drake, D. M., Spence, T., Gontijo, S. M. L., Wells, P. G., & Allen, C. (2018). Hyperthermia-mediated drug delivery induces biological effects at the tumor and molecular levels that improve cisplatin efficacy in triple negative breast cancer. *Journal of Controlled Release*, *282*(January), 35–45. <https://doi.org/10.1016/j.jconrel.2018.04.029>
- Esposito, C. L., Cerchia, L., Catuogno, S., De Vita, G., Dassie, J. P., Santamaria, G., ... De Franciscis, V. (2014). Multifunctional aptamer-miRNA conjugates for targeted cancer therapy. *Molecular Therapy*, *22*(6), 1151–1163. <https://doi.org/10.1038/mt.2014.5>
- Gobbo, O. L., Sjaastad, K., Radomski, M. W., Volkov, Y., & Prina-Mello, A. (2015). Magnetic Nanoparticles in Cancer Theranostics. *Theranostics*, *5*(11), 1249–63. <https://doi.org/10.7150/thno.11544>
- Gold, L., Ayers, D., Bertino, J., Bock, C., Bock, A., Brody, E. N., ... Zichi, D. (2010). Aptamer-based multiplexed proteomic technology for biomarker discovery. *PLoS ONE*, *5*(12). <https://doi.org/10.1371/journal.pone.0015004>
- Hauser, A. K., Wydra, R. J., Stocke, N. A., Anderson, K. W., & Hilt, J. Z. (2015). Magnetic nanoparticles and nanocomposites for remote controlled therapies. *Journal of Controlled Release : Official Journal of the Controlled Release Society*, *219*, 76–94. <https://doi.org/10.1016/j.jconrel.2015.09.039>
- Hirshfield, K. M., & Ganesan, S. (2014). Triple-negative breast cancer. *Current Opinion in Obstetrics and Gynecology*, *26*(1), 34–40. <https://doi.org/10.1097/GCO.0000000000000038>
- Hoeflich, K. P., & Ikura, M. (2004). Radixin: Cytoskeletal adopter and signaling protein. *International Journal of Biochemistry and Cell Biology*, *36*(11), 2131–2136. <https://doi.org/10.1016/j.biocel.2003.11.018>
- Holliday, D. L & Speirs, V. (2011). Choosing the right cell line for breast cancer research. *Breast Cancer Research*, *215*(13). <https://doi.org/10.1007/s10549-008-0053-y>
- Howell, A., Anderson, A. S., Clarke, R. B., Duffy, S. W., Evans, D. G., Garcia-Closas, Gesher, A, J.,

## REFERENCES

- Key, T. J., Saxton, J. M., Harvie, M. N. (2014). Risk determination and prevention of breast cancer. *Breast Cancer Research : BCR*, *16*(5), 446. <https://doi.org/10.1186/s13058-014-0446-2>
- Issa, B., Obaidat, I. M., Albiss, B. A., & Haik, Y. (2013). Magnetic nanoparticles: surface effects and properties related to biomedicine applications. *International Journal of Molecular Sciences*, *14*(11), 21266–305. <https://doi.org/10.3390/ijms141121266>
- Itoh, T., Erdmann, K. S., Roux, A., Habermann, B., Werner, H., & De Camilli, P. (2005). Dynamin and the actin cytoskeleton cooperatively regulate plasma membrane invagination by BAR and F-BAR proteins. *Developmental Cell*, *9*(6), 791–804. <https://doi.org/10.1016/j.devcel.2005.11.005>
- Jo, H., Her, J., & Ban, C. (2015). Dual aptamer-functionalized silica nanoparticles for the highly sensitive detection of breast cancer. *Biosensors and Bioelectronics*, *71*, 129–136. <https://doi.org/10.1016/j.bios.2015.04.030>
- Kim, D., Jeong, Y. Y., & Jon, S. (2010). A Drug Loaded Aptamer-Gold Nanoparticle Bioconjugate for Combined CT Imaging and Therapy of Prostate Cancer, *4*(7), 10–12. <https://doi.org/10.1021/nn901877h>
- Koltzschner, M., Neumann, C., Kö, S., & Gerke, V. (2003). Clint: A Novel Clathrin-binding ENTH-Domain Protein at the Golgi. *Molecular Biology of the Cell*, *14*(February), 2372–2384. <https://doi.org/10.1091/mbc.E02-03-0171>
- Ku, T., Zhang, T., Luo, H., Yen, T. M., Chen, P., Han, Y., & Lo, Y. (2015). Nucleic Acid Aptamers: An Emerging Tool for Biotechnology and Biomedical Sensing. *Sensors*, 16281–16313. <https://doi.org/10.3390/s150716281>
- Kuo, W. S., Chang, C. N., Chang, Y. T., Yang, M. H., Chien, Y. H., Chen, S. J., & Yeh, C. S. (2010). Gold nanorods in photodynamic therapy, as hyperthermia agents, and in near-infrared optical imaging. *Angewandte Chemie - International Edition*, *49*(15), 2711–2715. <https://doi.org/10.1002/anie.200906927>

- Lehmann, B. D., Bauer, J. A., Chen, X., Sanders, M. E., Chakravarthy, A. B., Shyr, Y., & Pietenpol, J. A. (2011). Identification of human triple-negative breast cancer subtypes and preclinical models for selection of targeted therapies. *The Journal of Clinical Investigation*, *121*(7), 2750–67. <https://doi.org/10.1172/JCI45014>
- Lehmann, B. D., Jovanović, B., Chen, X., Estrada, M. V., Johnson, K. N., Shyr, Y., Moses, H. L., Sanders, M. E., Pietenpol, J. A. (2016). Refinement of Triple-Negative Breast Cancer Molecular Subtypes: Implications for Neoadjuvant Chemotherapy Selection. *PLOS ONE*, *11*(6), e0157368. <https://doi.org/10.1371/journal.pone.0157368>
- Li, J., Zheng, H., Bates, P. J., Malik, T., Li, X. F., Trent, J. O., & Ng, C. K. (2014). Aptamer imaging with Cu-64 labeled AS1411: Preliminary assessment in lung cancer. *Nuclear Medicine and Biology*, *41*(2), 179–185. <https://doi.org/10.1016/j.nucmedbio.2013.10.008>
- Li, N., Larson, T., Nguyen, H. H., Sokolov, K. V., & Ellington, A. D. (2010). Directed evolution of gold nanoparticle delivery to cells. *Chemical Communications*, *46*(3), 392–394. <https://doi.org/10.1039/b920865h>
- Li, W., Bing, T., Wei, J., Chen, Z., Shangguan, D., & Fang, J. (2014). Biomaterials Cell-SELEX-based selection of aptamers that recognize distinct targets on metastatic colorectal cancer cells. *Biomaterials*, *35*(25), 6998–7007. <https://doi.org/10.1016/j.biomaterials.2014.04.112>
- Li, X., Zhang, W., Liu, L., Zhu, Z., Ouyang, G., An, Y., Zhao, C., Yang, C. J. (2014). In Vitro Selection of DNA Aptamers for Metastatic Breast Cancer Cell Recognition and Tissue Imaging.
- Linder, S., Hüfner, K., Wintergerst, U., & Aepfelbacher, M. (2000). Microtubule-dependent formation of podosomal adhesion structures in primary human macrophages. *Journal of Cell Science*, *113 Pt 23*, 4165–76. Retrieved from <http://www.ncbi.nlm.nih.gov/pubmed/11069762>

## REFERENCES

- Liu, Q., Wang, Y., Fang, X., Zhang, X., Chen, Z., & Tan, W. (2014). Aptamer-conjugated nanomaterials for specific cancer cell recognition and targeted cancer therapy. *Asia Materials*, 6(4). <https://doi.org/10.1038/am.2014.12>
- Ma, H., Liu, J., Ali, M. M., Mahmood, M. A. I., Labanieh, L., Lu, M., Iqbal, S. M., Zhang, Q., Zao & W., Wan, Y. (2015). Nucleic acid aptamers in cancer research, diagnosis and therapy. *Chemical Society Reviews*, 44, 1240–1256. <https://doi.org/10.1039/C4CS00357H>
- Mann, A. P., Bhavane, R. C., Somasunderam, A., Montalvo-Ortiz, B. L., Ghaghada, K. B., Volk, D., Nieves-Alicea, R., Suh, K. S., Ferrari, M., Annapragada, A., Gorenstein, D. G. & Tanaka, T. (2011). Thioaptamer Conjugated Liposomes for Tumor Vasculature Targeting. *Oncotarget*, 2(4), 298–304. <https://doi.org/10.18632/oncotarget.261>
- Mayer, I. A., Abramson, V. G., Lehmann, B. D., & Pietenpol, J. A. (2014). New strategies for triple-negative breast cancer-deciphering the heterogeneity. *Clinical Cancer Research*, 20(4), 782–790. <https://doi.org/10.1158/1078-0432.CCR-13-0583>
- McNamara, J. O., Andrechek, E. R., Wang, Y., Viles, K. D., Rempel, R. E., Gilboa, E., Sullenger, B. A. & Giangrande, P. H. (2006). Cell type-specific delivery of siRNAs with aptamer-siRNA chimeras. *Nature Biotechnology*, 24(8), 1005–1015. <https://doi.org/10.1038/nbt1223>
- Mendes, T. F. S., Kluskens, L. D., & Rodrigues, L. R. (2015). Triple Negative Breast Cancer: Nanosolutions for a Big Challenge. *Advanced Science*, 2(11), 1–14. <https://doi.org/10.1002/advs.201500053>
- Meng, H., Fu, T., Zhang, X., & Tan, W. (2015). Cell-SELEX-based aptamer-conjugated nanomaterials for cancer diagnosis and therapy. *National Science Review*, 2, 71–84. <https://doi.org/10.1093/nsr/nwv001>
- Meng, H., Xue, M., Xia, T., Zhao, Y.-L., Tamanoi, F., Stoddart, J. F., Zink, J. I. & Nel, A. E. (2010). Autonomous in vitro anticancer drug release from mesoporous silica nanoparticles by pH-sensitive nanovalves. *Journal of the American Chemical Society*, 132(36), 12690–12697. <https://doi.org/10.1021/ja104501a>



- Miller-Kleinhenz, J. M., Bozeman, E. N., & Yang, L. (2015). Targeted Nanoparticles for Image-guided Treatment of Triple Negative Breast Cancer: Clinical Significance and Technological Advances. *Wiley Interdiscip Rev Nanomed Nanobiotechnol*, *7*(6), 797–816.  
<https://doi.org/10.1161/CIRCRESAHA.116.303790>.The
- Mills, I. G., Praefcke, G. J. K., Vallis, Y., Peter, B. J., Olesen, L. E., Gallop, J. L., Butler, P. J. G., Evans, P. R. & McMahon, H. T. (2003). Epsinr: An AP1/clathrin interacting protein involved in vesicle trafficking. *Journal of Cell Biology*, *160*(2), 213–222.  
<https://doi.org/10.1083/jcb.200208023>
- Modrejewski, J., Walter, J.-G., Kretschmer, I., Kemal, E., Green, M., Belhadj, H., Blume, C. & Scheper, T. (2016). Aptamer-modified polymer nanoparticles for targeted drug delivery. *BioNanoMaterials*, *17*(1–2), 43–51. <https://doi.org/10.1515/bnm-2015-0027>
- Nakatsuka, M. A., Mattrey, R. F., Esener, S. C., Cha, J. N., & Goodwin, A. P. (2012). Aptamer-crosslinked microbubbles: Smart contrast agents for thrombin-activated ultrasound imaging. *Advanced Materials*, *24*(45), 6010–6016. <https://doi.org/10.1002/adma.201201484>
- Nass, S. J., Henderson, I. C., & Lashof, J. C. (2001). *Mammography and Beyond: Developing Technologies for the Early Detection of Breast Cancer Committee on Technologies for the Early Detection of Breast Cancer* (Vol. 6). Washington (DC). Retrieved from <http://www.nap.edu/catalog/10030.html>
- Nobrega, F. L., Ferreira, D., Martins, I. M., Suarez-Diez, M., Azeredo, J., Kluskens, L. D., & Rodrigues, L. R. (2016). Screening and characterization of novel specific peptides targeting MDA-MB-231 claudin-low breast carcinoma by computer-aided phage display methodologies. *BMC Cancer*, *16*(1), 881. <https://doi.org/10.1186/s12885-016-2937-2>
- Oh, N., & Park, J. H. (2014). Endocytosis and exocytosis of nanoparticles in mammalian cells. *International Journal of Nanomedicine*, *9*(SUPPL.1), 51–63.  
<https://doi.org/10.2147/IJN.S26592>
- Opazo, F., Levy, M., Byrom, M., Schäfer, C., Geisler, C., Groemer, T. W., ... Rizzoli, S. O. (2012). Aptamers as potential tools for super-resolution microscopy. *Nature Methods*, *9*(10), 938–

## REFERENCES

939. <https://doi.org/10.1038/nmeth.2179>
- Orellana, E., & Kasinski, A. (2016). Sulforhodamine B (SRB) Assay in Cell Culture to Investigate Cell Proliferation. *Bio-Protocol*, 6(21). <https://doi.org/10.21769/BioProtoc.1984>
- Pieve, C. Da, Perkins, A. C., & Missailidis, S. (2009). Anti-MUC1 aptamers: radiolabelling with <sup>99m</sup>Tc and biodistribution in MCF-7 tumour-bearing mice. *Nuclear Medicine and Biology*, 36(6), 703–710. <https://doi.org/10.1016/j.nucmedbio.2009.04.004>
- Prakash, J. S., & Rajamanickam, K. (2015). Aptamers and Their Significant Role in Cancer Therapy and Diagnosis. *Biomedicines*, 248–269. <https://doi.org/10.3390/biomedicines3030248>
- Puvanakrishnan, P., Diagaradjane, P., Kazmi, S. M. S., Dunn, A. K., Krishnan, S., & Tunnell, J. W. (2012). Narrow band imaging of squamous cell carcinoma tumors using topically delivered anti-EGFR antibody conjugated gold nanorods. *Lasers in Surgery and Medicine*, 44(4), 310–317. <https://doi.org/10.1002/lsm.22019>
- Qian, J., Chen, W., Lettau, M., Podda, G., Zörnig, M., Kabelitz, D., & Janssen, O. (2006). Regulation of FasL expression: A SH3 domain containing protein family involved in the lysosomal association of FasL. *Cellular Signalling*, 18(8), 1327–1337. <https://doi.org/10.1016/j.cellsig.2005.10.015>
- Savla, R., Taratula, O., Garbuzenko, O., & Minko, T. (2011). Tumor targeted quantum dot-mucin 1 aptamer-doxorubicin conjugate for imaging and treatment of cancer. *Journal of Controlled Release*, 153(1), 16–22. <https://doi.org/10.1016/j.jconrel.2011.02.015>
- Scholzen, T., & Gerdes, J. (2000). The Ki-67 Protein : From the Known and. *Journal of Cellular Physiology*, 322(August 1999), 311–322.
- Sefah, K., Shangguan, D., Xiong, X., O'Donoghue, M. B., & Tan, W. (2010). Development of DNA aptamers using Cell-SELEX. *Nature Protocols*, 5(6), 1169–1185. <https://doi.org/10.1038/nprot.2010.66>

- Silva, V. L., Ferreira, D., Nobrega, F. L., Martins, I. M., Kluskens, L. D., & Rodrigues, L. R. (2016). Selection of novel peptides homing the 4T1 cell line: Exploring alternative targets for triple negative breast cancer. *PLoS ONE*, *11*(8), 1–15. <https://doi.org/10.1371/journal.pone.0161290>
- Song, Y., Li, Y., Xu, Q., & Liu, Z. (2017). Mesoporous silica nanoparticles for stimuli-responsive controlled drug delivery: advances, challenges, and outlook. *International Journal of Nanomedicine*, *12*, 87–110. <https://doi.org/10.2147/IJN.S117495>
- Soule, H. D., Maloney, T. M., Wolman, S. R., Line, E. C., Peterson, W. D., Brenz, R., McGrath, C. M., Russo, J., Pauley, R. J., Jones, R. F. & Brooks, S. C. (1990). Isolation and Characterization of a Spontaneously Immortalized Human Breast. *Cancer*, 6075–6086.
- Stockmans, G., Deraedt, K., Wildiers, H., Moerman, P., & Paridaens, R. (2008). Triple-negative breast cancer. *Current Opinion in Oncology*, *20*(6), 614–620. <https://doi.org/10.1097/CCO.0b013e328312efba>
- Wan, Y., Tamuly, D., Allen, P. B., Kim, Y., Bachoo, R., Ellington, A. D., & Iqbal, S. M. (2014). Proliferation and Migration of Tumor Cells in Tapered Channels Biomed Microdevices. *Biomedical Microdevices*, *15*(4), 635–643. <https://doi.org/10.1007/s10544-012-9721-0>
- Wang, G., Liu, J., Chen, K., Xu, Y., Liu, B., Liao, J., Zhu, L., Hu, X., Li, J., Pu, Y., Fu, T. Liu, H & Tan, W. (2017). Selection and characterization of DNA aptamer against glucagon receptor by cell-SELEX. *Scientific Reports*, *7*(1), 1–10. <https://doi.org/10.1038/s41598-017-05840-w>
- Wang, Z., Tian, Y., Zhang, H., Qin, Y., Li, D., Gan, L., & Wu, F. (2016). Using hyaluronic acid-functionalized pH stimuli-responsive mesoporous silica nanoparticles for targeted delivery to CD44-overexpressing cancer cells. *International Journal of Nanomedicine*, *11*, 6485–6497. <https://doi.org/10.2147/IJN.S117184>
- Wu, X., Shaikh, A., Yu, Y., Li, Y., Ni, S., Lu, A., & Zhang, G. (2017). Potential Diagnostic and Therapeutic Applications of Oligonucleotide Aptamers in Breast Cancer. *International*

## REFERENCES

- Journal of Molecular Sciences*, 18(12), 1851. <https://doi.org/10.3390/ijms18091851>
- Wullner, U., Neef, I., Eller, A., Kleines, M., Tur, M., & Barth, S. (2008). Cell-Specific Induction of Apoptosis by Rationally Designed Bivalent Aptamer-siRNA Transcripts Silencing Eukaryotic Elongation Factor 2. *Current Cancer Drug Targets*, 8(7), 554–565.  
<https://doi.org/10.2174/156800908786241078>
- Yallapu, M. M., Othman, S. F., Curtis, E. T., Gupta, B. K., Jaggi, M., & Chauhan, S. C. (2011). Multi-functional magnetic nanoparticles for magnetic resonance imaging and cancer therapy. *Biomaterials*, 32(7), 1890–905.  
<https://doi.org/10.1016/j.biomaterials.2010.11.028>
- Yingchoncharoen, P., Kalinowski, D. S., & Richardson, D. R. (2016). Lipid-based drug delivery systems in cancer therapy: What is available and what is yet to come. *Pharmacological Reviews*, 68(3), 701–787. <https://doi.org/10.1124/pr.115.012070>
- Zheng, J., Zhu, G., Li, Y., Li, C., & You, M. (2013). A Spherical Nucleic Acids Platform Based on Self-Assembled DNA Biopolymer for High Performance Cancer Therapy. *ACS Nano*, 7(8), 6545–6554. <https://doi.org/10.1021/nn402344v>
- Zhou, J., & Rossi, J. (2017). Aptamers as targeted therapeutics: Current potential and challenges. *Nature Reviews Drug Discovery*, 16(3), 181–202.  
<https://doi.org/10.1038/nrd.2016.199>
- Zhu, G., Ye, M., Donovan, M. J., Song, E., Zhao, Z., & Tan, W. (2012). Nucleic acid aptamers: an emerging frontier in cancer therapy. *Chemical Communications*, 48(85), 10472.  
<https://doi.org/10.1039/c2cc35042d>

### Web Pages:

American Type Culture Collection. (n.d.). MDA-MB-231 ATCC® HTB-26™. Retrieved June 19, 2017, from [https://www.lgcstandards-atcc.org/Products/All/HTB-26.aspx?geo\\_country=pt#characteristics](https://www.lgcstandards-atcc.org/Products/All/HTB-26.aspx?geo_country=pt#characteristics)

- Helbig, I. (2015). STXBP1 – this is what you need to know in 2015 | Beyond the Ion Channel. Retrieved August 17, 2018, from <http://epilepsygenetics.net/2015/08/04/stxbp1-this-is-what-you-need-to-know-in-2015/>
- Smolke Lab, S. B. (n.d.). Phenol-chloroform vs. columns - smolke laboratory. Retrieved July 30, 2018, from <http://smolkelab.weebly.com/phenol-chloroform-vs-columns.html>

**Books:**

- Nelson, D., & Cox, M (2005). Lehninger principles of biochemistry (4th ed.):. *Biochemistry and Molecular Biology Education*, 33(1). <https://doi.org/10.1002/bmb.2005.494033010419>
- Brown, T. A. (2002). The Human Genome. In *Genomes 2* (2nd ed.). Wiley-Liss. Retrieved from <https://www.ncbi.nlm.nih.gov/books/NBK21134/>

**Supplier Sheets:**

- Installation, E. (2017). sicastar®-greenF COOH Technical data sheet, 66–67.



## APPENDIXES





## Bradford Protein Assay

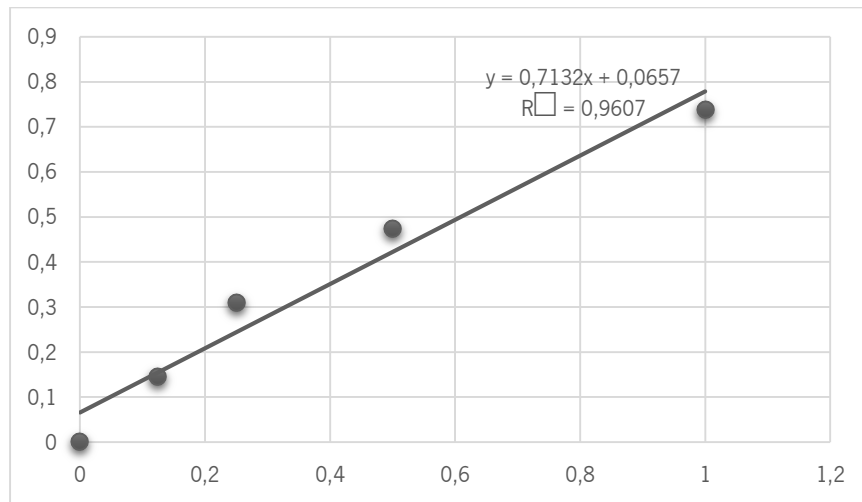


Figure A.1 Calibration curve of Bradford Protein Assay.  $y = 0,7132x + 0,0657$ ;  $R^2 = 0,9607$

## Aptamer mediated pull-down assay

SDS-PAGE gels from assays using BSA and FBS

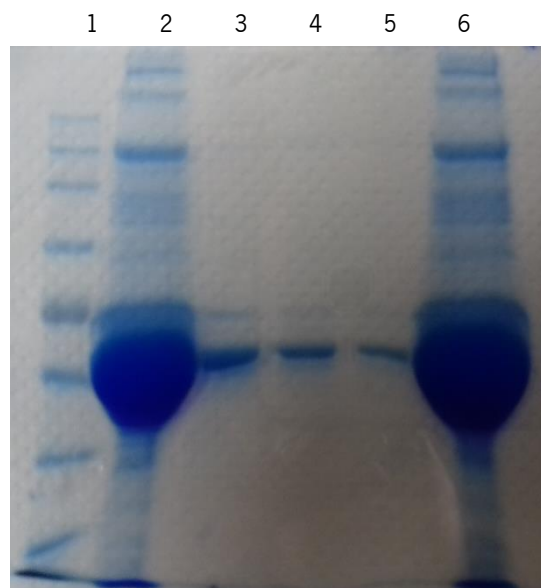
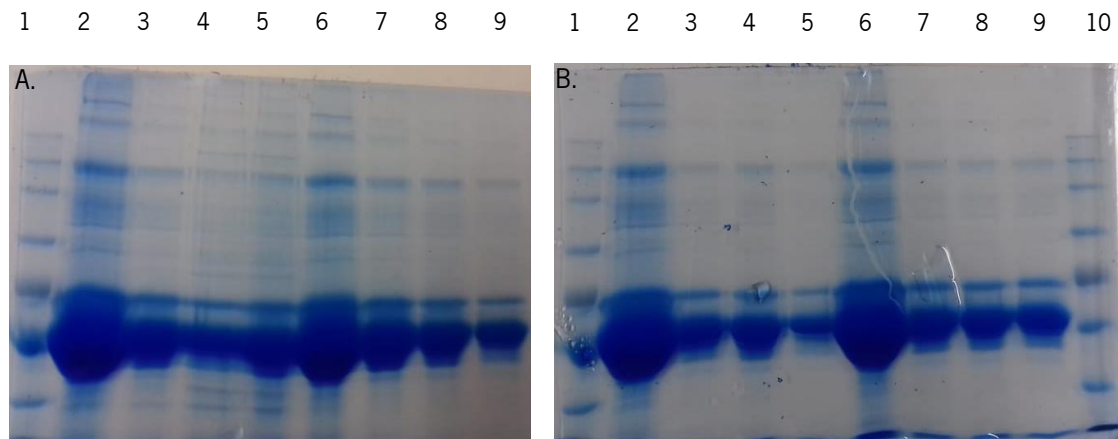


Figure A.2 Aptamer #1 mediated pull down assay of membrane fraction using Binding Buffer containing FBS and BSA. (1) Biomarker, (2 and 6) membrane fraction, (3) membrane fraction incubated with beads, (4) membrane fraction incubated with aptamer at 4 °C and (5) membrane fraction incubated with aptamer at 37 °C.

APPENDIXES



**Figure A.3** Aptamer #1 mediated pull-down assay of (A) nuclear, mitochondrial, (B) cytosolic and membrane fraction using Binding Buffer containing FBS. A: (1) Biomarker, (2) nuclear fraction, (3) nuclear fraction incubated with beads, (4) nuclear fraction incubated with aptamer at 4 °C, (5) nuclear fraction incubated with aptamer at 37 °C, (6) mitochondrial fraction, (7) mitochondrial fraction incubated with beads, (8) mitochondrial fraction incubated with aptamer at 4 °C, (9) mitochondrial fraction incubated with aptamer at 37 °C. B (1) Biomarker, (2) cytosol fraction, (3) cytosol fraction incubated with beads, (4) cytosol fraction incubated with aptamer at 4 °C, (5) cytosol fraction incubated with aptamer at 37 °C, (6) membrane fraction, (7) membrane fraction incubated with beads, (8) membrane fraction incubated with aptamer at 4 °C, (9) membrane fraction incubated with aptamer at 37 °C and (10) Biomarker.